Geol. Mag. **148** (*3*), *2011, pp. 380–403. © Cambridge University Press 2010*
doi:10.1017/S0016756810000804

Sinistral transport along the Trans-European Suture Zone: detrital zircon–rutile geochronology and sandstone petrography from the Carboniferous flysch of the Pontides

NİLGÜN OKAY*†, THOMAS ZACK‡, ARAL I. OKAY§ & MATTHIAS BARTH‡

*İstanbul Teknik Üniversitesi, Maden Fakültesi, Jeoloji Müh. Bölümü, Maslak 34469 İstanbul, Turkey
‡Institut für Geowissenschaften, Universität Mainz, Becherweg 21, 55128 Mainz, Germany
§İstanbul Teknik Üniversitesi, Avrasya Yerbilimleri Enstitüsü, Maslak 34469 İstanbul, Turkey

(*Received* 3 January 2010; *accepted* 22 June 2010; *first published online* 29 September 2010)

Abstract – The Lower Carboniferous flysch of the Istanbul Zone in Turkey is an over 1500 m thick turbiditic sandstone–shale sequence marking the onset of the Variscan deformation in the Pontides. It overlies Lower Carboniferous black cherts and is unconformably overlain by Lower Triassic continental sandstones and conglomerates. The petrography of the Carboniferous sandstones and the geochronology and geochemistry of the detrital zircons and rutiles were studied to establish the provenance of the clastic rocks. The sandstones are feldspathic to lithic greywackes and subgreywackes with approximately equal amounts of quartz, feldspar and lithic clasts. The amount of quartz and lithic fragments decreases upwards in the sequence at the expense of feldspar. The lithic fragments are dominated by intermediate volcanic rocks, followed by metamorphic and sedimentary rock fragments. Coarse lithic fragments are generally granitoidic. In the discrimination diagrams, sandstone samples lie mainly in the field of dissected arc. A total of 218 detrital zircons and 35 detrital rutiles from four sandstone samples were analysed with laser ablation ICP-MS. The detrital zircons show a predominantly bimodal age distribution with Late Devonian to Early Carboniferous (390 to 335 Ma) and Cambrian–Neoproterozoic (640 to 520 Ma) ages. The remaining 9 % of the analysed zircons are in the 1700–2750 Ma range; zircons of the 700–1700 Ma age range are absent. The REE patterns and Th/U ratios of the zircons are consistent with a magmatic origin. With one exception (Neoproterozoic), the rutile ages are Late Devonian–Early Carboniferous and their geochemistry indicates that they were derived from amphibolite-facies metamorphic rocks. Sandstone petrography and detrital zircon–rutile ages suggest one dominant source for the Lower Carboniferous sandstones: a Late Devonian to Early Carboniferous magmatic and metamorphic province with overprinted Neoproterozoic basement. Late Devonian–Early Carboniferous magmatic and metamorphic rocks are unknown from the Eastern Mediterranean region. They are, however, widespread in central Europe. The Istanbul Zone is commonly correlated with the Avalonian terrranes in central Europe, which collided with the Armorican terranes during Carboniferous times, resulting in the Variscan orogeny. The Carboniferous flysch of the Istanbul Zone must have been derived from a colliding Armorican terrane, as indicated by the absence of 700–1700 Ma zircons and by Late Devonian–Early Carboniferous magmatism, typical features of the Armorican terranes. This suggests that during Carboniferous times the Istanbul terrane was located close to the Bohemian Massif and has been translated by strike-slip along the Trans-European Suture Zone to its Cretaceous position north of the Black Sea.

Keywords: Carboniferous flysch, Istanbul Zone, Pontides, detrital zircon geochronology, detrital rutile geochronology, sandstone petrography, Trans-European Suture Zone.

1. Introduction

The Lower Carboniferous flysch (Culm flysch) of the Istanbul Zone is an over 1500 m thick turbiditic sandstone–shale sequence marking the onset of the Variscan deformation in the Pontides. It forms the highest stratigraphic unit in the 5 km thick Ordovician to Carboniferous sedimentary sequence, deposited on a long-standing passive continental margin south of Laurussia. The Istanbul Palaeozoic sequence of the Pontides has been compared and correlated with similar sequences in central and western Europe, including the Moesian platform in Romania and Bulgaria, Moravo-Silesia (Brunovistulian) in the Czech Republic and the Rhenohercynian zone in Germany and Belgium (e.g. Pharaoh, 1999; Kalvoda *et al.* 2003, 2008; Sunal *et al*. 2008), all deposited on the northern passive margin of the Rheic ocean. The closure of the Rheic ocean and the ensuing collision with the Armorican terrane assemblage in the Carboniferous led to the Variscan deformation (e.g. Tait *et al*. 1997). The Variscan deformation was the last major orogenic event in Central Europe, therefore the provenance of the Devonian–Carboniferous turbidites in Central Europe can be confidently traced to distinct terranes (e.g. Schäfer *et al.* 1997). In contrast, the Pontides were affected by the Triassic and Early Tertiary closures of the Palaeo- and Neotethyan oceans, respectively, and

†Author for correspondence: okayn@itu.edu.tr

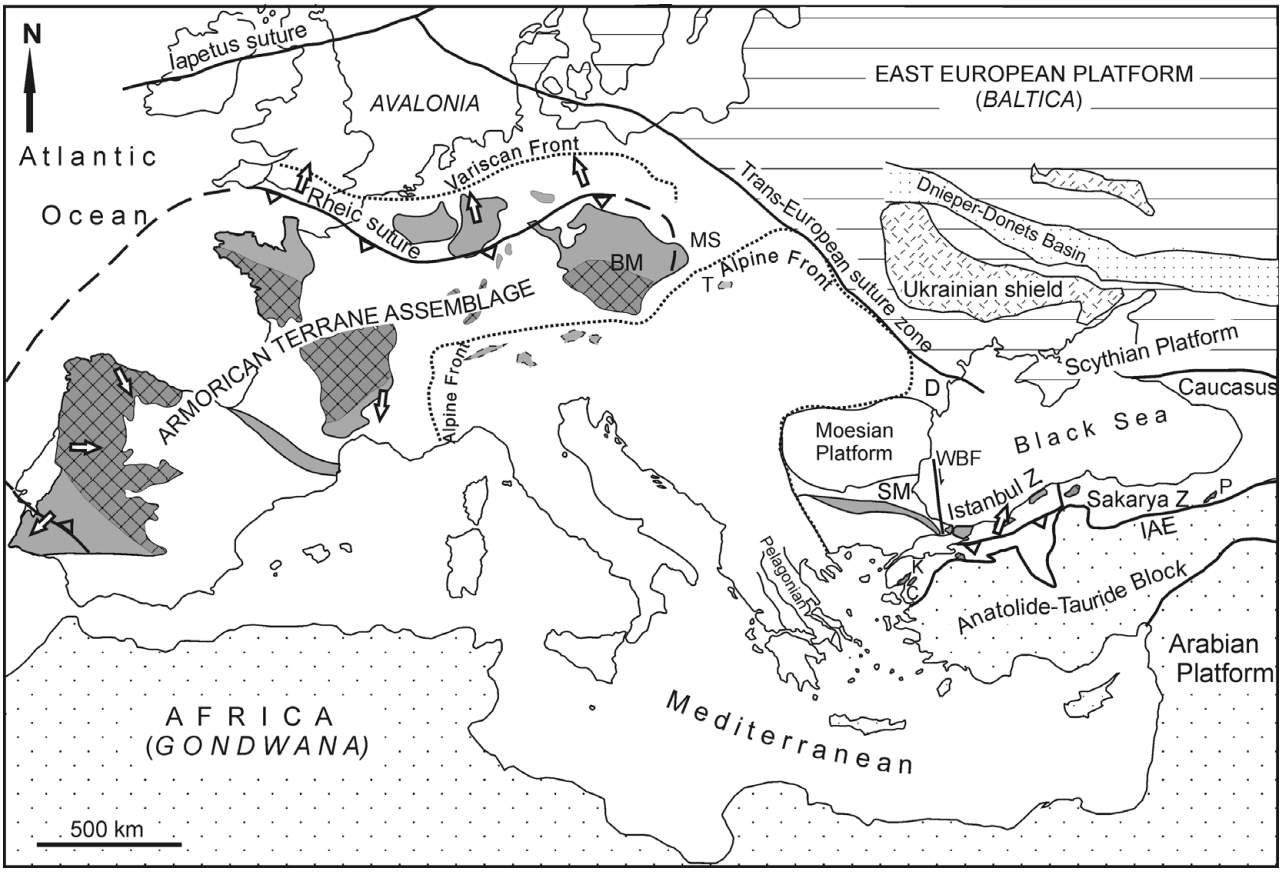

Figure 1. Simplified tectonic map of Europe showing the Variscan units. The cross-hatched pattern indicates regions with medium- to high-grade Carboniferous metamorphism. The triangles on the sutures indicate subduction polarities and the arrows the vergence of Variscan deformation. BM – Bohemian Massif; Ç – Çamlık granitoid; D – Dobrugea; K – Kazdağ Massif; MS – Moravo-Silesia; IAE – Izmir–Ankara–Erzincan suture; P – Pulur Massif; SM – Strandja Massif; T – Tatra mountains; WBF – West Black Sea Fault (modified after Okay *et al.* 2008).

the resultant Cimmeride and Alpide deformations, so that the Carboniferous flysch of the Pontides has no obvious provenance in the adjacent tectonic zones. The Istanbul Zone is a good example of a small crustal fragment within younger sequences that is difficult to set into a solid geodynamic context. In this study we use sandstone framework petrography, detrital zircon and rutile geochronology and geochemistry to reconstruct the provenance of the Carboniferous flysch of the Pontides, and hence to trace the origin of the Istanbul Zone.

2. Geological setting

The Pontides consist of three terranes amalgamated during Cretaceous times (Okay & Tüysüz, 1999). These are the Strandja, Istanbul and Sakarya zones (Fig. 1). The Istanbul Zone, located along the southwestern Black Sea coast, consists of a Precambrian crystalline basement overlain by a continuous, well-developed transgressive sedimentary sequence extending from Ordovician to Carboniferous (Fig. 2; Görür *et al.* 1997). The Palaeozoic sequence was folded and possibly thrust-faulted during the Late Carboniferous Hercynian orogeny, and is unconformably overlain by Lower Triassic and younger sedimentary strata. The Istanbul Zone is separated from the Sakarya Zone by the Intra-Pontide suture and from the Strandja Massif by the right-lateral strike-slip West Black Sea Fault (Fig. 3). The Sakarya and Strandja terranes exhibit Late Triassic and Late Jurassic–Early Cretaceous metamorphism and deformation, respectively, which are not observed in the Istanbul Zone.

3. The stratigraphy of the Istanbul Zone

3.a. Precambrian basement

The crystalline basement of the Istanbul Zone crops out widely in the Bolu Massif, with smaller outcrop areas in the Karadere and in the Armutlu peninsula (Fig. 3). The basement is divided into four units (Ustaömer & Rogers, 1999; Yiğitbaş *et al.* 2004): (a) a metamorphic sequence dominated by quartzo-feldspathic gneiss and amphibolite; (b) a disrupted mafic–ultramafic sequence consisting of amphibolite, metapyroxenite, metaperidotite and metagabbro; (c) meta-andesites with minor metarhyolites and metasedimentary rocks; (d) voluminous intrusive granitoids. The plutons, which make up more than half of the basement, are Neoproterozoic (590–560 Ma) calc-alkaline tonalites to granodiorites (Chen *et al.* 2002; Ustaömer, Mundil &

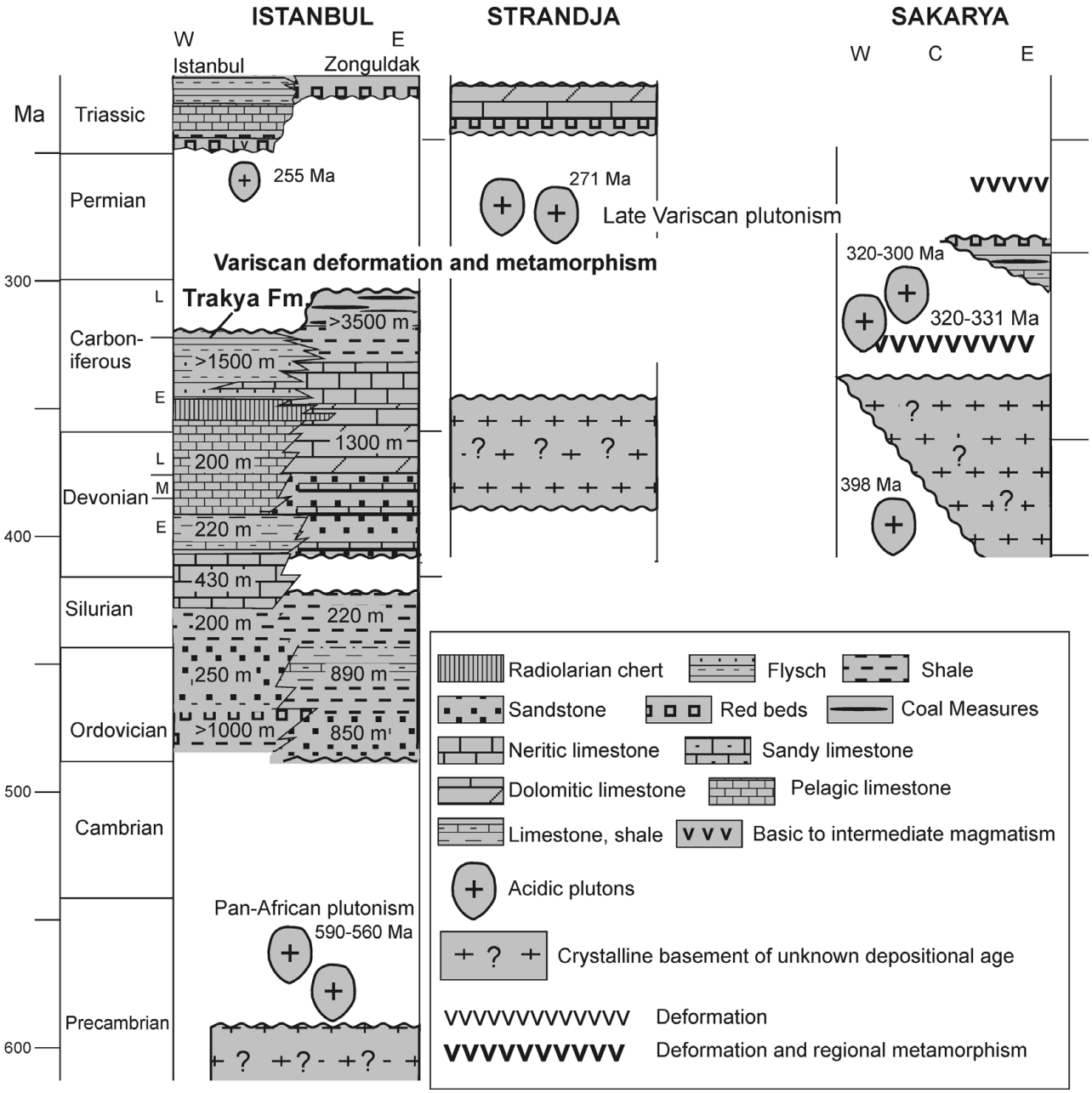

Figure 2. Stratigraphic columns of the Pontide terranes showing the major plutonic and metamorphic events (modified from Okay, Satır & Siebel, 2006).

Renne, 2005; Okay *et al.* 2008). The Rb/Sr biotite ages from the Karadere basement are 548–545 Ma, showing that the basement was not heated above 300 °C after the latest Proterozoic (Chen *et al.* 2002).

3.b. The Palaeozoic series in the western part of the Istanbul Zone

The well-developed Palaeozoic series around Istanbul have been studied since the middle of the 20th century (e.g. Paeckelmann, 1938; Okay, 1947; Kaya, 1969; Haas, 1968; Ustaömer *et al.* 2010). They form an exclusively sedimentary sequence, more than 5 km thick, extending from Ordovician to Carboniferous (Fig. 2).

In the Istanbul region the lowermost exposed Palaeozoic rocks are violet to pinkish fluvial arkosic sandstone, conglomerate and minor shale, more than 1000 m thick, exposed over large regions in the Asian part of the city of Istanbul (Fig. 4). These continental clastics, assumed to be Ordovician in age, are overlain by white cross-bedded quartzites, locally with ripple marks, 200–300 m thick, deposited in a tide-dominated shore environment. The quartzites pass laterally and vertically into a sequence of greywacke, siltstone and shale, 200 m thick, deposited in a lagoonal to shallow marine environment. The upper parts of this Gözdağ Formation include a chamosite–oolite horizon with Lower Silurian (Llandoverian) brachiopods, ostrocods, corals and conodonts (Haas, 1968). The Gözdağ Formation is overlain by a shallow marine carbonate sequence of Middle to Late Silurian (Wenlock and Ludlow) to Early Devonian (Sieganian)

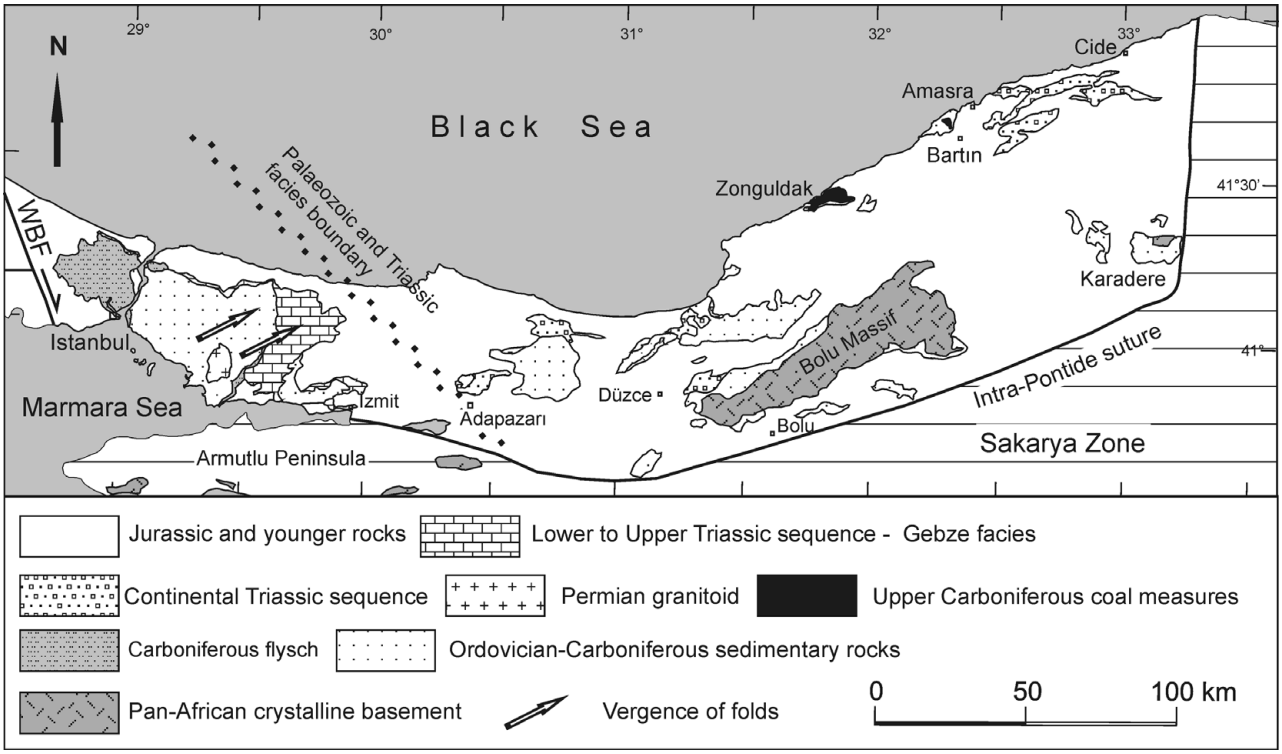

Figure 3. The distribution of pre-Jurassic rocks in the Istanbul Zone (simplified from Türkecan & Yurtsever, 2002, and Aksay *et al.* 2002). Note the different Carboniferous and Triassic facies in the western and eastern parts of the Istanbul Zone, and the trend of the facies boundary, which is highly oblique to the Intra-Pontide suture (modified after Okay, Satır & Siebel, 2006). WBF – West Black Sea Fault.

age. The carbonates indicate an increasingly deepening marine environment towards the southeast (Haas, 1968). The limestones pass up into richly fossiliferous shales and siltstones of latest Early Devonian (late Emsian) age, which are in turn overlain by thinly to irregularly banded marly nodular limestones, marls and shales of latest Early Devonian (Late Emsian) to earliest Carboniferous (Tournaisian) age, deposited in deep water (Çapkınoğlu, 2000, 2005; Göncüoğlu, Boncheva & Göncüoğlu, 2004). Above the nodular limestone comes a characteristic horizon, 40 m thick, of black Middle to Late Tournaisian radiolarian cherts intercalated with shales containing phosphatic nodules (Okay, 1947; Noble *et al.* 2008). The radiolarian cherts are overlain by siliciclastic turbidites of the Trakya Formation, over 1500 m in thickness. In the lower part of the Trakya Formation, there are tongues of *in situ* shallow-marine upper Visean bioclastic limestones (Kaya & Mamet, 1971). The Trakya Formation is overlain unconformably by the lowermost Triassic red sandstones and conglomerates.

3.c. The Palaeozoic sequence in the eastern part of the Istanbul Zone

In the eastern part of the Istanbul Zone in the Karadere region, sandstones with possible early Ordovician (Tremodacian) acritarchs lie unconformably over the crystalline basement (Dean *et al.* 2000). The sandstones are overlain sharply by quartzites, which pass up to a black mudstone–shale series with local horizons rich in Ordovician (early Arenig to Llanvirn) graptolites (Fig. 2). The mudstones are overlain by dark limestones with shale and siltstone intercalations with Ordovician (Caradoc) conodonts. The Silurian is represented by black shales with graptolites and acritarchs indicative of the Llandovery and Wenlock (Dean *et al.* 2000). The Devonian carbonates lie over the Silurian with an angular unconformity (Boztuğ, 1992).

The upper parts of the Palaeozoic succession are best exposed around the city of Zonguldak. The succession starts with Upper Devonian (Frasnian–Famennian) neritic carbonates, which pass up without interruption into Tournaisian dolomite reef limestones and Visean shallow marine carbonates and shales (Dil, 1976). The uppermost Visean consists of alternating limestones and shales, and grades into the Namurian black shales. These are overlain by coal-bearing lacustrine, fluviatile and fluviomarine clastic rocks, ~ 3500 m in thickness and of Namurian and Westphalian age. The clastics were deposited in large south-facing deltas on the margin of Laurussia (Kerey, 1984; Kerey, Kelling & Wagner, 1986).

The stratigraphic differences between the western and eastern parts of the Istanbul Zone are best interpreted as a result of lateral facies changes. Analogous Palaeozoic facies differences exist in the Polish Variscan zones (e.g. Narkiewicz, 2007), in the Brunovistulian (Kalvoda *et al.* 2003; Kalvoda & Bábek, 2010), in the Hercynian of Europe between the Ardennes and the Rheinisches Schiefergebirge (e.g. Rutten, 1969, p. 115) and in the Moesian Platform, where neritic

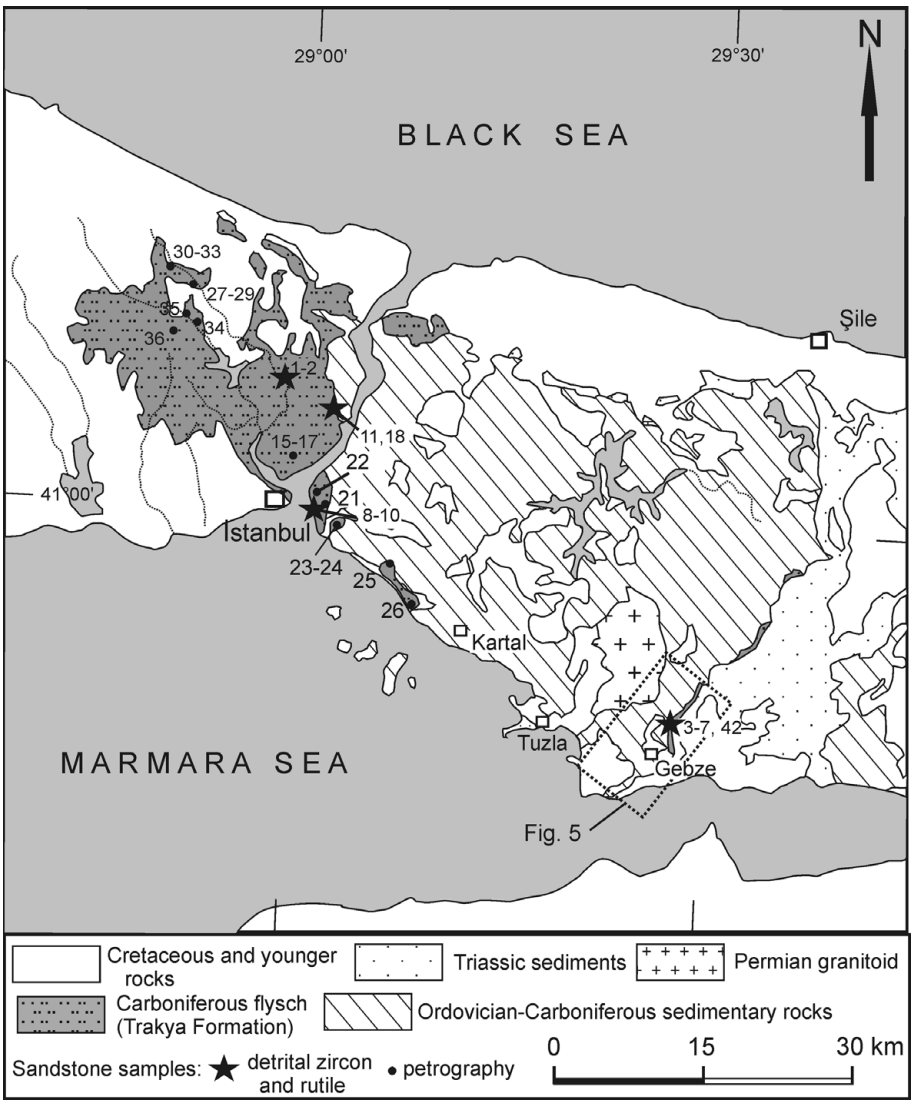

Figure 4. Simplified geological map of the Istanbul region showing the outcrops of the Carboniferous flysch and the sample localities (modified from Türkecan & Yurtsever, 2002). For location, see Figure 3.

carbonate deposition in the Tournaisian in the north is replaced by radiolarian chert sedimentation in the south in the Elovitza region (Haydoutov & Yanev, 1997).

3.d. Late Carboniferous deformation and Early Permian plutonism

The Palaeozoic deposition in the Istanbul region ends in the Early Carboniferous and is followed by shortening deformation with the generation of recumbent folding, local cleavage and minor thrusting. The minor folds generally show an E–NE vergence (Zapcı, Akyüz & Sunal, 2003); however, the age of the structures, whether Variscan or later, is not well constrained. Nevertheless, the observation that the lowermost Triassic red beds step down from Carboniferous to Ordovician (Fig. 5) indicates significant deformation, uplift and erosion in the Late Carboniferous–Permian interval. The deformed Palaeozoic rocks are intruded by a Permian granite east of Istanbul with early Late Permian (*c.* 255 Ma) zircon U–Pb and biotite K–Ar ages (Yılmaz, 1977; Şahin *et al*. 2009). In the Zonguldak region the Palaeozoic sequence extends into the Upper Carboniferous (Westphalian) coal measures, followed by thrust-faulting and folding. Several of the coal seams in the Zonguldak basin are inverted (Loboziak & Dill, 1973).

4. Carboniferous flysch: the Trakya Formation

The Trakya Formation consists predominantly of an alternation of sandstone, siltstone and shale. It is the highest stratigraphic unit of the Istanbul Palaeozoic sequence (Paeckelmann, 1938; Kaya, 1969, 1971) and underlies most of the city of Istanbul, especially west of the Bosphorus (Fig. 4). Sandstone beds are thicker and more frequent in the lower parts of the sequence (Fig. 6a); the upper part of the sequence consists of millimetre-scale parallel-laminated, fine-grained, dark sandstones, siltstones and shales with 5–20 cm thick bedding (Fig. 6b). This facies, exposed in large quarries, can form packages up to 50 m thick. Within

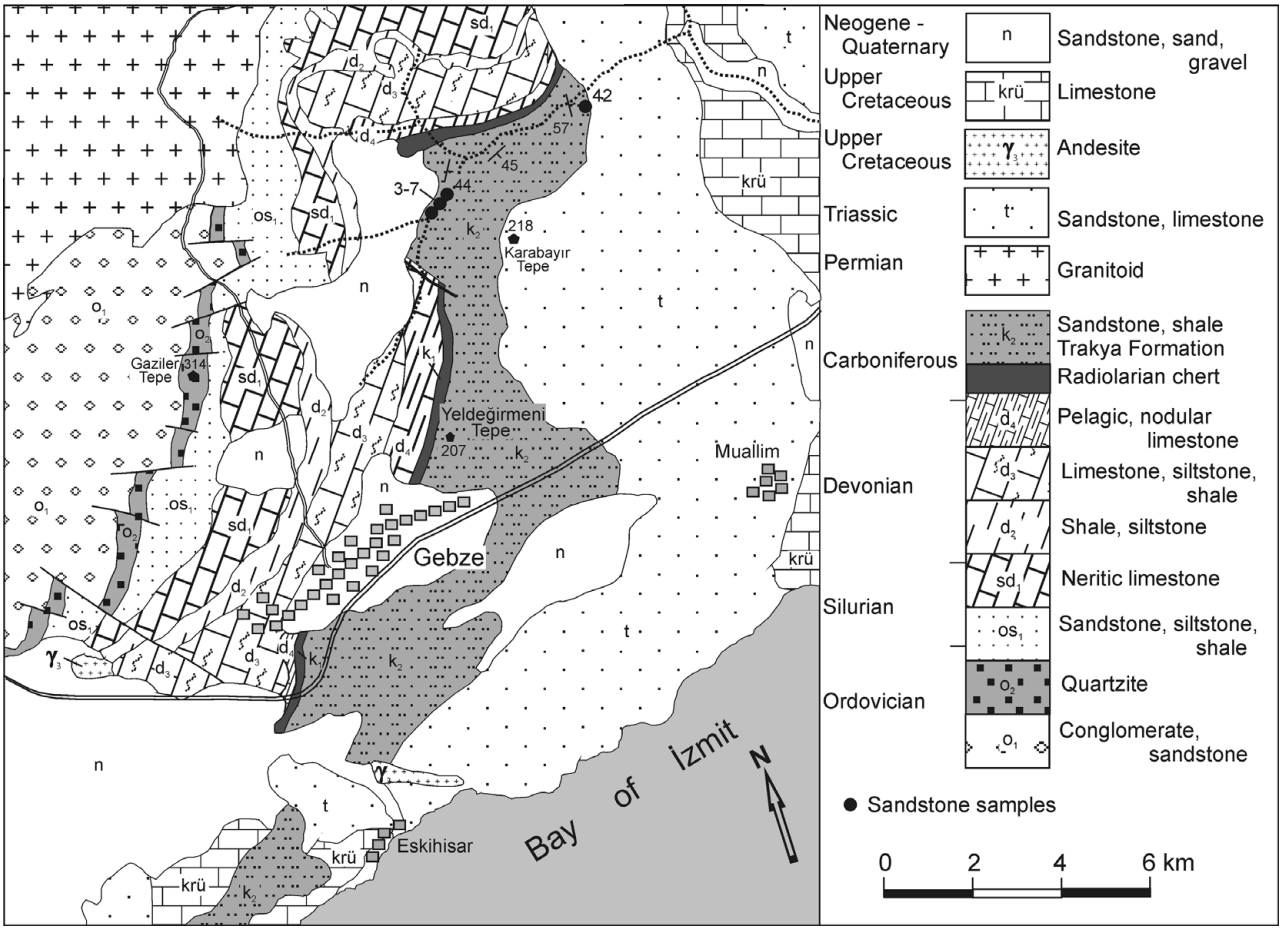

Figure 5. Geological map of the Gebze region (modified from Ketin, 1983). Note the erosional truncation of the Palaeozoic sequence at the base of the Triassic series. Location of the sandstone samples is indicated. For location, see Figure 4.

this laminated facies there are coarse- to medium-grained, dark-grey sheet sandstones, which range up to 2 m in bed thickness, with sharp erosive bases. Such sandstones may be massive or normally graded. The sedimentological features of the Trakya Formation indicate deposition from turbidity currents.

The Trakya Formation is deformed by folding and intense faulting. Slaty cleavage is locally observed in the siltstones and shales but has not developed in the sandstones, which are generally free of penetrative deformation. Apatite fission track studies show that the Trakya Formation has experienced temperatures of above 120 °C (M. Zattin, pers. comm.); however, quartz grains in the sandstones show no evidence of recrystallization, indicating that the burial temperatures did not exceed ~ 300 °C.

5. Petrography and detrital modes of the Carboniferous sandstones

We sampled thickly to medium-bedded, medium- to coarse-grained sandstone beds for petrography. In most outcrops the sandstones are yellowish brown due to the oxidation of the chlorite-rich matrix and alteration of unstable lithic fragments; we chose grey to dark-grey fresh sandstones from quarries, road sections and drill cores. Because of deformation and scarcity of continuous outcrops, the relative stratigraphic position of most of the samples is not clear. The exception is the Gebze region east of Istanbul, where a ~ 200 m section from the base of the Trakya Formation above the Tournaisian radiolarian cherts was sampled (Fig. 5). The Gebze samples represent the basal parts of the Trakya Formation, whereas the rest of the samples come from its middle and upper parts.

Compositional data from sandstone point counts were collected from 21 samples. The location of the samples is shown in Figures 4 and 5 and their coordinates are given in Table 1. The point-counted sandstones were free of penetrative strain and recrystallization. The petrographic thin-sections were stained with potassium rhodizonate for plagioclase and with sodium cobaltinitrite for potassium feldspar identifications, respectively. However, almost all the plagioclase is albite and there is very little potassium feldspar in the sandstones. The point counting was done using the Gazzi–Dickinson method (e.g. Dickinson, 1970; Ingersoll *et al.* 1984), whereby sand-sized (> 0.03 mm) monominerallic components of lithic fragments are counted as individual mineral grains, and only aphanitic grains (< 0.03 mm) are classed as lithic fragments. More than 400 framework grains were identified in each section. The indeterminate grains average less than 3 % of the total count. Petrographic

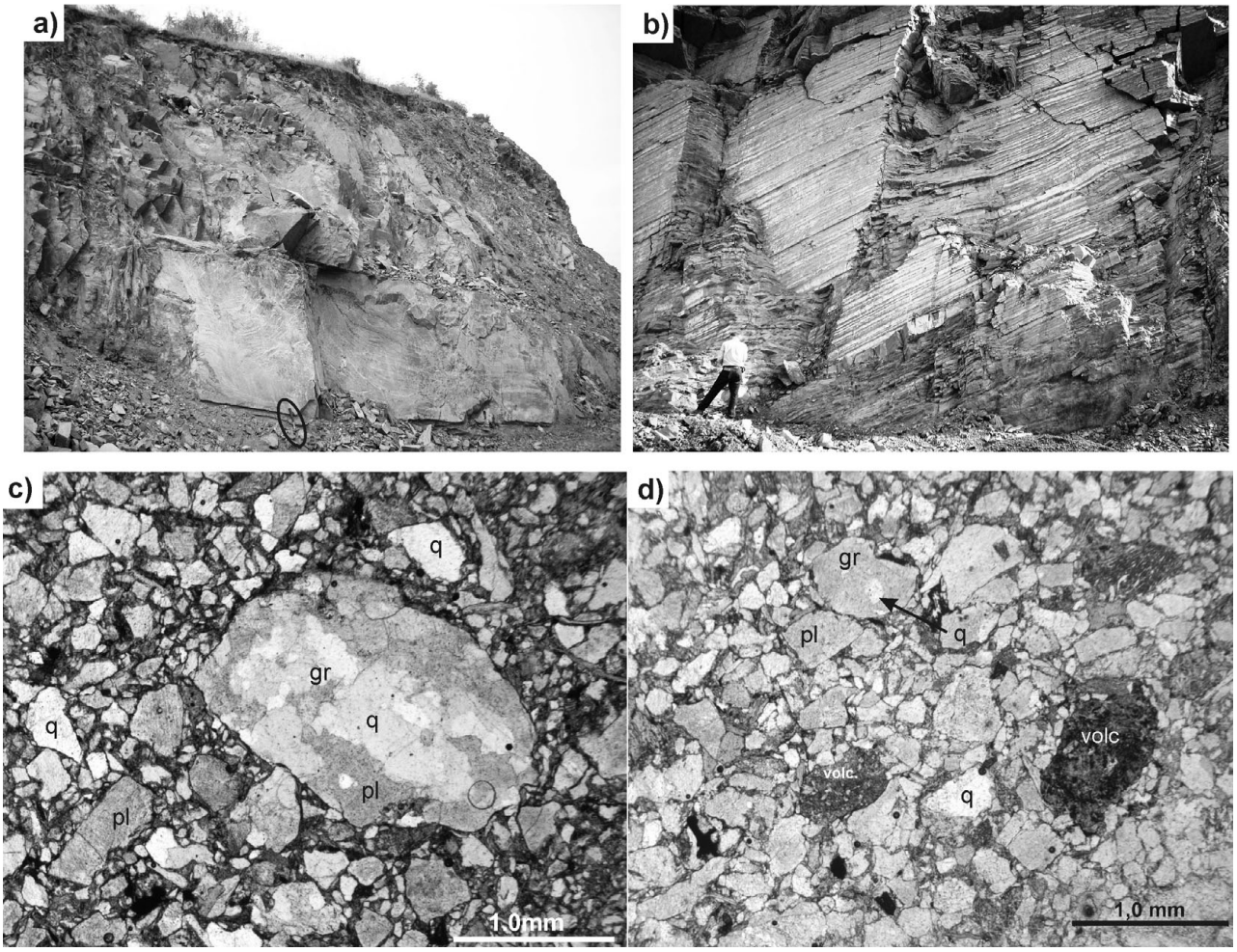

Figure 6. (a) Thickly-bedded feldspar-rich sandstones from the basal parts of the Trakya Formation from the Gebze region. Hammer for scale is 32 cm long. (b) Rhythmically interbedded fine-grained sandstone, siltstone and shale, which characterizes most of the Trakya Formation. Person is 180 cm tall. (c, d) Photomicrographs from the sandstones of the Trakya Formation. All in plane polarized light. (c) Large granitic clast (gr) with quartz (q) and plagioclase (pl). The euhedral shapes of some plagioclase grains in the matrix indicate a magmatic origin. Note the poor sorting and the abundance of the matrix, sample 7. (d) Volcanic clasts and a small granitic fragment; again note the euhedral shape of the plagioclase grains, sample 3.

counting parameters and modal point-count data are presented in Table 1.

Petrographically the sandstones of the Trakya Formation are feldspathic to lithic greywackes and subgreywackes (Pettijohn, Potter & Siever, 1987). They are poorly sorted and consist of angular to subangular grains in a voluminous matrix (Fig. 6c, d). The matrix, defined as grains less than 0.03 mm across, makes up between 12 and 22 % of the rock (Table 1). It is chlorite rich but also contains silt-size particles of feldspar and quartz. In some cases it is difficult to differentiate between the 'matrix' and deformed and diagenetically altered very fine-grained volcanic lithic grains.

The sandstones from the Trakya Formation generally consist of approximately equal amounts of feldspar, quartz and lithic fragments (Fig. 7). Quartz forms individual monocrystalline grains with irregular outlines. It is also found as globular, oval inclusions in plagioclase crystals in granitoidic clasts (Fig. 6c). Polycrystalline quartz is rare and consists mainly of fine-grained quartzite. Plagioclase has two modes of origin. Coarse-grained subhedral to euhedral crystals are derived from a magmatic protolith, as also shown by the presence of individual plagioclase crystals in granitic and volcanic clasts (Fig. 6c, 6d). Rounded plagioclase grains with oriented inclusions have been derived from metamorphic rocks.

The most common lithic grains are slightly metamorphic fine-grained andesite to trachyte consisting of murky chlorite, feldspar and leucoxene (Fig. 6d). A yellowish brown palagonitized and chloritized volcanic glass is common in sandstones from the Gebze region. Second in abundance are metamorphic rock grains, mainly phyllite, muscovite-schist, chlorite-schist and quartz-micaschist (Fig. 7b). The sedimentary lithic fragments are rare and include quartzite, slate and siltstone; carbonate grains are very scarce. Calcite, present in a few samples, is of secondary origin and occurs as veins or replaces feldspar. Detrital chlorite and muscovite are common but minor constituents, making up a few per cent each (Table 1).

Sandstones from the Gebze region from the lower parts of the Trakya Formation are rich in feldspar, which makes up 50–60 % of the grains. The average sandstone

Table 1. Locations and modal compositions of Carboniferous sandstones

Sample					QQmQpFL%				LvLmLs%				
No.	Field no.	Mode	UTM coordinates	n	Q	Qm	Qp	F	L	Lv	Lm	Ls	m
1A	106	rc	35T 0665612–4554034	664	48	42	6	35	17	50	38	12	18
1B	106	rc	35T 0665612–4554034	667	45	39	6	30	26	52	39	9	16
3	111	q	35T 0707539–4523121	785	30	27	2	55	15	66	32	2	16
4	112	rc	35T 0707613–4523149	496	26	25	0	58	17	63	8	29	13
5	113	rc	35T 0707656–4523154	408	22	21	2	59	18	63	8	29	15
6	114	rc	35T 0707700–4523157	613	25	24	1	56	19	77	4	19	11
7	115	rc	35T 0707771–4523167	902	28	28	1	53	19	95	5	0	13
8	116	rc	35T 0669263–4542076	462	49	42	7	31	19	86	9	5	22
9	117	rc	35T 0669231–4542229	648	41	38	3	30	29	59	41	0	17
10	118	rc	35T 0669024–4542817	726	44	42	2	29	28	57	34	9	13
11b	121B	rc	35T 0670830–4551987	534	41	44	3	28	24	78	19	4	22
15	7A	c-42 m	35T 0669360–4548350	614	44	35	9	28	28	68	32	0	12
16	1A	c-28 m	35T 0669368–4548345	722	42	38	4	34	24	59	41	0	14
18	B9	rc	35T 0670863–4554260	904	47	43	4	26	27	79	20	1	19
19	123	c-40 m	35T 0670125–4539880	735	31	30	2	48	24	56	43	1	17
21	125	c-15 m	35T 0669950–4542450	688	42	37	5	32	26	51	44	5	16
22	126	c-13 m	35T 0670050–4541625	601	34	32	3	37	29	60	40	0	15
24	127B	c-14 m	35T 0671510–4539745	647	44	36	8	31	25	94	4	2	19
25	128	c-12 m	35T 0676510–4536350	701	42	36	7	29	29	85	13	2	17
26	129	c-8 m	35T 0679500–4533200	641	41	36	6	22	36	88	10	2	15
42	151	rc	35T 0709636–4523975	654	28	24	3	53	19	73	17	10	13
Istanbul average					43	38	5	29	26	68	28	4	16
Gebze average					26	25	2	56	18	73	12	15	14

rc – road cut; q – quarry; c-15 m – core sample at 15 m depth; Q – total quartz; Qm – monocrystalline quartz; Qp – polycrystalline quartz; F – feldspar; L – rock fragments; Lv – volcanic; Lm – metamorphic Ls – sedimentary rock fragments; n – number of point counts; m – matrix

composition in the Gebze region is $Q_{26}F_{56}L_{18}$, whereas the average sandstone composition from the other regions is $Q_{43}F_{29}L_{26}$ (Table 1). The amount of plagioclase appears to decrease upwards in the sequence at the expense of quartz with minor enrichment in lithic grains (Fig. 7).

The framework modal data from the Carboniferous sandstones plot near the centre of the Q–F–L diagram, mainly within the deeply eroded or dissected magmatic arc field with minor overlap to the recycled orogenic field (Fig. 7a). A magmatic arc provenance is also indicated by the volcanic–metamorphic–sedimentary lithic diagram (Fig. 7b), and by the Qp–Lvm–Lsm (polycrystalline quartz – volcanic + metavolcanic lithics – sedimentary + metasedimentary lithics) diagram (Ingersoll & Suczek, 1979).

Microconglomerates and pebbly sandstones make up less than 1 % of the Trakya Formation. They are found as 1–3 m thick beds associated with coarse-grained sandstones. The clasts in the conglomerates are well-rounded, polished and covered with a brown tarnish; they range in size from a few millimetres to 10 cm. Observations in three separate conglomerate outcrops (coordinates: 35T 06 54 380 – 45 63 218, 35T 06 56 672–45 62 337, 35T 06 55 483 – 45 54 674) have shown that ~ 80 % of the clasts consist of quartz, the rest are quartz-micaschist, granitoid and sandstone.

6. Detrital zircon and rutile geochronology

6.a. Methods

Four sandstone samples, two from the Asian side of the Bosphorus (Gebze-3 and Scutaria-8) and two from the European side (Maslak-1B and 18) were chosen for detrital zircon and rutile analysis. Zircons and rutiles were extracted using standard techniques involving crushing, sieving, heavy liquid separation and hand-picking. The zircon and rutile separates were mounted in epoxy, ground to expose cores of crystals and polished, and were analysed using Laser Ablation Inductively Coupled Plasma Mass Spectrometry (LA-ICP-MS) in the Institut für Geowissenschaften, Johannes Gutenberg-Universität Mainz, using a New Wave Research UP-213 (wavelength 213 nm) laser system combined with an Agilent 7500ce quadrupole-ICP mass spectrometer (LA-Q-ICP-MS).

For zircon U–Pb analysis, purification of the zircon surface was achieved by pre-ablating the analysis spot with five laser shots with a beam diameter larger than the analysis spots. Each analysis consists of a background measurement of 40 seconds, followed by 30 seconds of sample analysis. The U–Pb data were collected by ablating zircons with a laser beam diameter of 40–50 μm, a beam energy density of about 3.5 J/cm^2, and a repetition rate of 10 Hz. The aerosol produced during ablation was transported to the ICP-MS in a mixed Ar–He carrier gas at a flow rate of 1.3 l/minute. Isotopes were measured in time-resolved mode. Dwell times for each isotope of individual mass scans are 10 ms for ^{232}Th and ^{238}U, 30 ms for ^{201}Hg, ^{204}Hg+Pb and ^{206}Pb, and 50 ms for ^{207}Pb and ^{208}Pb. Th and U concentrations, ^{206}Pb/^{204}Pb ratios, as well as ^{207}Pb–^{235}U, ^{206}Pb–^{238}U and ^{208}Pb–^{232}Th ages were calculated off-line from time-resolved raw counts. No common Pb correction was made because of the imprecise ^{206}Pb/^{204}Pb ratios. The zircon standard

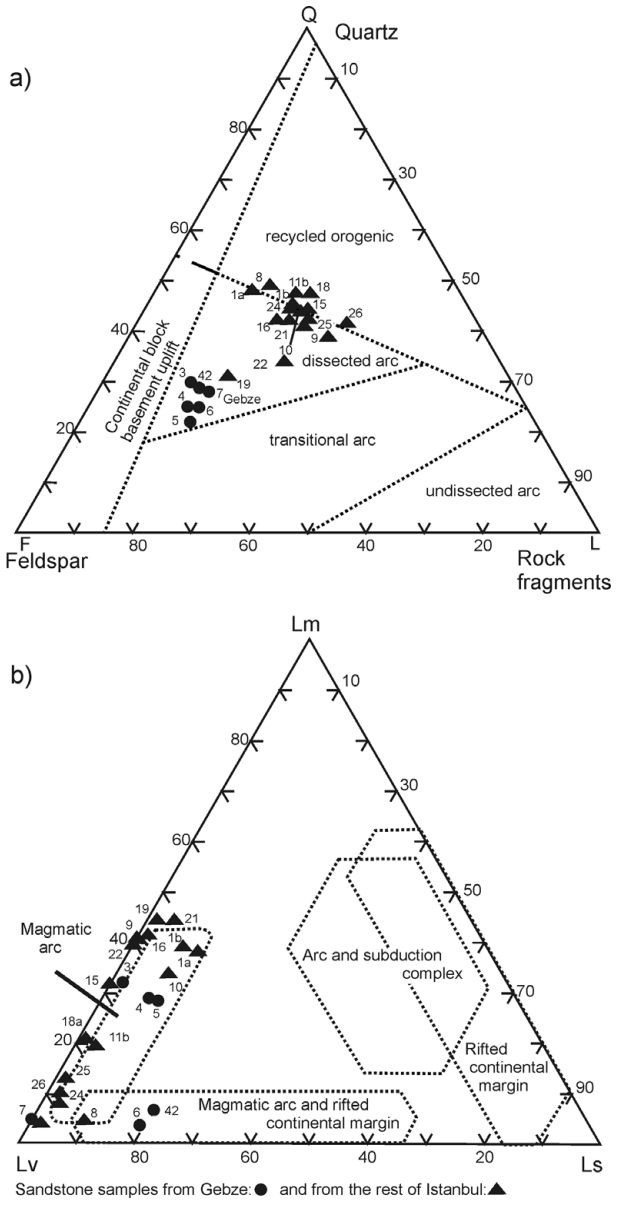

Figure 7. Sandstone compositional data from the Trakya Formation plotted on ternary diagrams. (a) Q–F–L provenance discrimination diagram (Dickinson *et al.* 1983). (b) Volcanic, metamorphic and sedimentary lithic components and provenance (Ingersoll & Suczek, 1979).

PL (Plesovice; 337.1 ± 0.4 Ma; Slama *et al.* 2008) was used as a primary standard to correct for laser-induced as well as ICP-induced mass fractionation by integrating the same time segments for each sample and standard zircon (Jackson *et al.* 2004). The accuracy of ages cannot currently be better determined than ~ 2 %, based on long-term reproducibility of the zircon standards GJ-1, which was also used to calculate U and Th concentrations (Jackson *et al.* 2004), 91500 (Wiedenbeck *et al.* 1995) and Mud Tank (Black & Gulson, 1978).

Rutiles were analysed closely following the procedure described in Zack *et al*. (in press). Here, trace elements (V, Cr, Zr, Nb, Sn, Hf, Ta, W and U) were determined first by ablating material from 10 μm diameter spots. These results were not only used to determine rock type and metamorphic temperatures (see Section 7), but also to find high-U rutiles suitable for LA-Q-ICP-MS dating. In a second run, rutiles with U concentrations > 5 ppm were analysed for U–Pb age determinations employing a laser beam of 50 μm after cleaning the surface with 70 μm laser shots. Isotopes and dwell times are identical to zircon setup. The rutile standard R10 (1090 ± 5 Ma; Luvizotto *et al*. 2009) was used as a primary standard. In contrast to zircon dating, $^{206}Pb/^{208}Pb$ ratios can be used for a very robust and reliable common Pb correction, due to the fact that rutiles are generally extremely Th-poor (see Zack *et al*. in press for further details). Comparison with another rutile standard (R19; 489.5 ± 0.9 Ma; Zack *et al*. in press) reveals that accuracy is currently limited to ~ 2 %.

6.b. Results

A total of 234 detrital zircons from four samples were dated, which assures that no important fraction (> 5 %) of the zircon age population is missed (e.g. Vermeesch, 2004). Sixteen zircon analyses were discarded due to irregular ablation signals. The remaining 218 zircons are apparently concordant and are considered further (Table 2). For the correlation of isotopic and stratigraphic ages we use the geological time scale of Gradstein *et al.* (2004).

Zircons from the Carboniferous sandstone samples show predominantly a bimodal age distribution, with Cambrian–Neoproterozoic (520 to 640 Ma; 49 % of all zircons) and Late Devonian–Early Carboniferous (335–390 Ma; 42 %) ages (Fig. 8a). Zircons of these ages are euhedral to subhedral and mostly show oscillatory and rarely sector zoning (Fig. 9), consistent with a magmatic source. Apart from these two dominant groups, there is a small population of Silurian–Ordovician ages (425–485 Ma; 2 %). The third largest population consists of 14 Palaeoproterozoic to Archaean zircons (1700–2700 Ma; 6 %). These zircons are rounded and generally show a gradual zoning (Fig. 9), suggesting a more complex history. The most striking pattern is the absence of zircon ages between 700 and 1700 Ma, characteristic for terranes derived from West Africa and Armorica (Fig. 10, Nance & Murphy, 1994; Linneman *et al*. 2004).

Zircons from sample Gebze-3, stratigraphically the lowermost sample, are dominantly earliest Carboniferous (*c*. 359 Ma, 52 zircons), with only 13 Cambrian–Neoproterozoic zircons (Figs 11a, 12a). Samples Scutaria-8 and Maslak-18 yielded approximately equal numbers of earliest Carboniferous (38 zircons) and Cambrian–Neoproterozoic zircons (24 zircons); the sample Maslak-1B contains predominantly Cambrian–Neoproterozoic zircons (49 zircons) with only two earliest Carboniferous (358 Ma) zircons (Fig. 11c).

The Late Devonian–Early Carboniferous zircons exhibit a narrow age range; the concordia ages for the Gebze-3 and Scutaria-8 zircon samples can be assumed to belong to one age group, where pooled ages are

Table 2. U–Pb isotope data from the detrital zircons from the Carboniferous sandstones of the Istanbul Zone

No.	U ppm	Th ppm	Th/U ratio	$^{206}Pb/^{204}Pb$ ratio	$^{207}Pb/^{235}U$ ratio	1s	$^{206}Pb/^{238}U$ ratio	1s	σ	$^{207}Pb/^{206}Pb$ ratio	1s	$^{207}Pb/^{235}U$ Ma	1s	$^{206}Pb/^{238}U$ Ma	1s
Sample 3 – Gebze															
1	149	189	0.79	>1105	0.405	0.067	0.0543	0.0014	0.13	0.0543	0.0089	345	50	341	8
2	187	725	0.26	5043	0.412	0.022	0.0548	0.0027	0.55	0.0547	0.0027	351	16	344	17
3	164	438	0.37	>2900	0.393	0.013	0.0551	0.0018	0.53	0.0517	0.0016	337	9	346	11
4	143	259	0.55	>1734	0.402	0.013	0.0552	0.0016	0.45	0.0528	0.0017	343	10	346	10
5	84	96	0.87	243	0.447	0.021	0.0555	0.0021	0.38	0.0584	0.0028	375	15	348	13
6	672	542	0.81	3323	0.408	0.010	0.0558	0.0013	0.75	0.0531	0.0009	347	7	350	8
7	267	199	0.75	>1113	0.415	0.012	0.0559	0.0011	0.57	0.0538	0.0013	352	9	351	6
8	735	616	0.84	>2815	0.415	0.008	0.0561	0.0007	0.72	0.0537	0.0008	353	6	352	4
9	316	214	0.68	>1253	0.419	0.010	0.0561	0.0009	0.59	0.0541	0.0011	355	7	352	5
10	409	195	0.48	2351	0.417	0.015	0.0561	0.0013	0.44	0.0539	0.0018	354	11	352	8
11	562	358	0.64	>2278	0.419	0.008	0.0562	0.0006	0.66	0.0540	0.0008	355	6	353	4
12	195	134	0.68	>950	0.404	0.011	0.0563	0.0008	0.48	0.0521	0.0013	345	8	353	5
13	256	169	0.66	1890	0.424	0.011	0.0564	0.0011	0.66	0.0546	0.0011	359	8	353	7
14	242	209	0.86	2009	0.418	0.010	0.0564	0.0010	0.62	0.0540	0.0011	355	7	354	6
15	238	159	0.67	>921	0.408	0.012	0.0566	0.0009	0.49	0.0522	0.0013	347	9	355	6
16	85	50	0.59	>526	0.423	0.014	0.0566	0.0014	0.42	0.0541	0.0018	358	10	355	8
17	134	100	0.74	>801	0.419	0.012	0.0567	0.0013	0.47	0.0536	0.0015	355	9	355	8
18	351	267	0.76	1562	0.421	0.011	0.0567	0.0009	0.59	0.0539	0.0011	357	8	355	6
19	263	206	0.78	1398	0.423	0.015	0.0569	0.0015	0.56	0.0539	0.0016	358	11	357	9
20	214	116	0.54	>878	0.417	0.013	0.0570	0.0013	0.51	0.0531	0.0015	354	10	357	8
21	143	82	0.57	>573	0.421	0.015	0.0570	0.0012	0.47	0.0536	0.0017	357	11	358	7
22	668	358	0.54	>2818	0.416	0.009	0.0571	0.0007	0.70	0.0529	0.0008	353	6	358	5
23	109	63	0.58	668	0.440	0.013	0.0572	0.0011	0.55	0.0559	0.0014	370	9	358	7
24	115	70	0.61	>436	0.431	0.015	0.0573	0.0011	0.40	0.0546	0.0018	364	11	359	7
25	1115	595	0.53	>4995	0.429	0.008	0.0573	0.0008	0.74	0.0543	0.0007	362	6	359	5
26	224	160	0.72	>1336	0.423	0.012	0.0574	0.0012	0.55	0.0536	0.0013	358	8	360	7
27	1299	995	0.77	7501	0.421	0.008	0.0574	0.0007	0.67	0.0532	0.0007	357	5	360	4
28	103	58	0.56	>533	0.432	0.030	0.0575	0.0030	0.42	0.0545	0.0037	365	21	360	19
29	220	167	0.76	>1450	0.433	0.011	0.0575	0.0010	0.59	0.0548	0.0011	365	8	360	6
30	715	421	0.59	3190	0.420	0.009	0.0575	0.0013	0.75	0.0530	0.0008	356	6	360	8
31	172	119	0.69	>1226	0.419	0.012	0.0575	0.0015	0.49	0.0528	0.0015	355	9	361	9
32	157	114	0.73	471	0.432	0.012	0.0576	0.0011	0.53	0.0546	0.0013	365	9	361	6
33	79	41	0.52	>530	0.425	0.015	0.0577	0.0013	0.35	0.0534	0.0019	359	11	361	8
34	135	77	0.57	>765	0.435	0.020	0.0577	0.0014	0.28	0.0547	0.0025	367	14	361	8
35	258	172	0.67	>1749	0.453	0.011	0.0577	0.0011	0.68	0.0571	0.0011	379	8	362	7
36	166	100	0.60	>616	0.416	0.013	0.0579	0.0007	0.36	0.0521	0.0015	353	9	363	4
37	105	66	0.64	>663	0.435	0.015	0.0580	0.0014	0.45	0.0544	0.0017	367	10	363	9
38	260	171	0.66	>1431	0.433	0.017	0.0580	0.0013	0.38	0.0541	0.0020	365	12	364	8
39	241	190	0.79	>1365	0.431	0.011	0.0581	0.0013	0.54	0.0538	0.0013	364	8	364	8
40	112	65	0.58	>598	0.418	0.021	0.0581	0.0016	0.30	0.0521	0.0025	354	15	364	10
41	769	675	0.88	>3151	0.427	0.009	0.0581	0.0008	0.72	0.0533	0.0008	361	6	364	5
42	108	68	0.64	>624	0.424	0.013	0.0582	0.0011	0.50	0.0529	0.0014	359	9	365	7
43	101	0	0.00	472	0.434	0.015	0.0582	0.0008	0.25	0.0540	0.0019	366	11	365	5
44	817	312	0.38	4019	0.461	0.016	0.0582	0.0013	0.47	0.0574	0.0018	385	12	365	8
45	146	100	0.69	>867	0.417	0.012	0.0583	0.0011	0.50	0.0520	0.0013	354	9	365	7
46	114	95	0.83	>700	0.441	0.015	0.0584	0.0012	0.46	0.0548	0.0017	371	11	366	7
47	152	109	0.72	>1003	0.430	0.013	0.0588	0.0015	0.55	0.0531	0.0014	363	9	368	9
48	319	189	0.59	2020	0.442	0.010	0.0592	0.0014	0.63	0.0541	0.0011	371	7	371	8
49	1006	432	0.43	>4442	0.444	0.011	0.0593	0.0011	0.68	0.0543	0.0010	373	8	371	7
50	199	202	1.02	>1472	0.432	0.013	0.0596	0.0016	0.48	0.0526	0.0015	365	9	373	9
51	374	260	0.69	>2286	0.451	0.015	0.0614	0.0019	0.50	0.0534	0.0017	378	11	384	11
52	184	98	0.53	>1378	0.453	0.011	0.0615	0.0014	0.55	0.0535	0.0012	380	8	385	8
53	701	628	0.90	>4533	0.679	0.018	0.0848	0.0018	0.67	0.0581	0.0011	526	11	524	11
54	380	219	0.58	>3450	0.719	0.017	0.0866	0.0018	0.64	0.0604	0.0011	550	10	535	11
55	423	146	0.35	>2676	0.722	0.016	0.0889	0.0015	0.69	0.0589	0.0010	552	10	549	9
56	412	220	0.53	>4038	0.755	0.018	0.0913	0.0019	0.66	0.0601	0.0011	571	10	563	11
57	33	58	0.57	>601	0.779	0.035	0.0915	0.0023	0.32	0.0617	0.0027	585	20	565	13
58	95	59	0.62	>591	0.803	0.027	0.0934	0.0021	0.49	0.0623	0.0019	598	16	576	12
59	382	147	0.38	2844	0.774	0.020	0.0948	0.0021	0.64	0.0592	0.0012	582	12	584	12
60	304	117	0.39	>2050	0.787	0.036	0.0952	0.0041	0.60	0.0599	0.0024	589	21	586	24
61	225	78	0.35	1005	0.775	0.027	0.0957	0.0028	0.56	0.0588	0.0018	583	15	589	16
62	72	46	0.63	>476	0.850	0.026	0.0979	0.0016	0.45	0.0629	0.0017	624	14	602	9
63	269	82	0.30	>1980	0.815	0.018	0.0980	0.0013	0.65	0.0603	0.0010	605	10	603	8
64	43	23	0.55	>439	0.899	0.034	0.0986	0.0021	0.42	0.0663	0.0023	651	18	606	12
65	35	21	0.59	>395	0.861	0.037	0.0989	0.0028	0.48	0.0633	0.0024	631	20	608	16
Sample 8 – Scutaria															
1	390	268	0.69	n.d.	0.415	0.006	0.0551	0.0006	0.20	0.0546	0.0009	353	5	346	3
2	259	252	0.98	n.d.	0.424	0.011	0.0553	0.0014	0.44	0.0555	0.0015	359	8	347	9
3	262	199	0.76	n.d.	0.411	0.015	0.0553	0.0009	0.39	0.0539	0.0018	350	11	347	6
4	118	89	0.76	n.d.	0.454	0.020	0.0555	0.0012	0.32	0.0592	0.0026	380	14	348	7
5	324	305	0.94	n.d.	0.413	0.007	0.0558	0.0007	0.26	0.0537	0.0010	351	5	350	4
6	269	246	0.91	n.d.	0.412	0.015	0.0560	0.0010	0.40	0.0534	0.0018	351	11	351	6
7	176	153	0.87	n.d.	0.420	0.008	0.0563	0.0005	0.11	0.0542	0.0011	356	6	353	3

Table 2. Continued.

No.	U ppm	Th ppm	Th/U ratio	$^{206}Pb/^{204}Pb$ ratio	$^{207}Pb/^{235}U$ ratio	1s	$^{206}Pb/^{238}U$ ratio	1s	σ	$^{207}Pb/^{206}Pb$ ratio	1s	$^{207}Pb/^{235}U$ Ma	1s	$^{206}Pb/^{238}U$ Ma	1s
8	286	258	0.90	n.d.	0.419	0.015	0.0563	0.0010	0.43	0.0540	0.0017	356	11	353	6
9	517	311	0.60	n.d.	0.417	0.015	0.0564	0.0011	0.43	0.0537	0.0018	354	11	354	7
10	184	121	0.66	n.d.	0.405	0.017	0.0564	0.0014	0.44	0.0521	0.0019	345	12	354	8
11	101	63	0.62	n.d.	0.434	0.019	0.0567	0.0010	0.31	0.0554	0.0024	366	14	356	6
12	577	491	0.85	n.d.	0.416	0.014	0.0568	0.0010	0.44	0.0532	0.0016	353	10	356	6
13	155	78	0.50	n.d.	0.430	0.010	0.0568	0.0006	0.11	0.0550	0.0014	364	7	356	3
14	109	71	0.65	n.d.	0.414	0.017	0.0568	0.0010	0.34	0.0529	0.0021	352	12	356	6
15	537	385	0.72	n.d.	0.414	0.014	0.0569	0.0010	0.41	0.0528	0.0016	352	10	356	6
16	102	83	0.81	n.d.	0.429	0.017	0.0571	0.0010	0.34	0.0545	0.0020	363	12	358	6
17	209	128	0.62	n.d.	0.421	0.015	0.0572	0.0010	0.40	0.0534	0.0018	357	11	358	6
18	234	151	0.64	n.d.	0.423	0.015	0.0574	0.0011	0.39	0.0535	0.0018	358	11	360	6
19	245	144	0.59	n.d.	0.424	0.016	0.0575	0.0012	0.42	0.0535	0.0019	359	12	361	7
20	419	245	0.59	n.d.	0.422	0.020	0.0575	0.0012	0.31	0.0531	0.0024	357	14	361	7
21	417	339	0.81	n.d.	0.427	0.015	0.0576	0.0011	0.39	0.0538	0.0018	361	11	361	7
22	194	165	0.85	n.d.	0.423	0.025	0.0577	0.0019	0.29	0.0531	0.0031	358	18	362	12
23	428	300	0.70	n.d.	0.428	0.006	0.0578	0.0005	0.15	0.0537	0.0008	361	4	362	3
24	123	114	0.92	n.d.	0.468	0.014	0.0580	0.0014	0.42	0.0585	0.0027	390	10	364	9
25	922	368	0.40	n.d.	0.436	0.018	0.0582	0.0018	0.48	0.0543	0.0021	367	13	365	11
26	191	109	0.57	n.d.	0.420	0.024	0.0583	0.0015	0.24	0.0523	0.0029	356	17	365	9
27	91	67	0.74	n.d.	0.438	0.029	0.0583	0.0016	0.23	0.0544	0.0036	369	21	366	10
28	175	101	0.58	n.d.	0.465	0.022	0.0585	0.0020	0.39	0.0577	0.0026	388	15	366	12
29	113	75	0.67	n.d.	0.486	0.030	0.0587	0.0016	0.29	0.0601	0.0036	402	21	368	10
30	399	252	0.63	n.d.	0.428	0.027	0.0595	0.0027	0.43	0.0522	0.0031	362	19	372	16
31	368	27	0.07	n.d.	0.462	0.017	0.0612	0.0012	0.44	0.0547	0.0018	386	12	383	8
32	403	61	0.15	n.d.	0.527	0.018	0.0681	0.0012	0.44	0.0561	0.0017	430	12	425	7
33	424	93	0.22	n.d.	0.530	0.028	0.0702	0.0021	0.30	0.0547	0.0028	431	18	438	13
34	112	39	0.35	n.d.	0.751	0.033	0.0844	0.0018	0.42	0.0646	0.0026	569	19	522	11
35	127	41	0.32	n.d.	0.692	0.025	0.0849	0.0015	0.38	0.0592	0.0020	534	15	525	9
36	288	96	0.33	n.d.	0.726	0.040	0.0860	0.0040	0.47	0.0612	0.0033	554	24	532	24
37	130	45	0.34	n.d.	0.830	0.043	0.0876	0.0036	0.44	0.0687	0.0035	614	24	542	21
38	208	66	0.32	n.d.	0.733	0.012	0.0892	0.0009	0.21	0.0596	0.0010	559	7	551	5
39	154	46	0.30	n.d.	0.805	0.077	0.0894	0.0081	0.49	0.0653	0.0062	600	44	552	48
40	389	76	0.20	n.d.	0.728	0.027	0.0895	0.0021	0.43	0.0590	0.0020	556	16	552	13
41	122	36	0.30	n.d.	0.789	0.016	0.0909	0.0011	0.25	0.0629	0.0013	590	9	561	6
42	403	215	0.53	n.d.	0.721	0.043	0.0915	0.0039	0.40	0.0572	0.0033	552	26	564	23
43	282	124	0.44	n.d.	0.750	0.026	0.0916	0.0017	0.43	0.0594	0.0019	568	15	565	10
44	115	35	0.30	n.d.	0.766	0.016	0.0919	0.0009	0.08	0.0604	0.0014	577	9	566	5
45	96	73	0.75	n.d.	0.810	0.020	0.092	0.002	0.50	0.0637	0.0027	602	12	568	13
46	168	55	0.33	n.d.	0.757	0.029	0.0928	0.0020	0.43	0.0591	0.0021	572	17	572	12
47	340	145	0.43	n.d.	0.769	0.027	0.0937	0.0017	0.45	0.0595	0.0018	579	15	577	10
48	98	70	0.72	n.d.	0.840	0.034	0.0941	0.0022	0.39	0.0648	0.0025	619	19	580	13
49	183	157	0.86	n.d.	0.799	0.030	0.0951	0.0021	0.39	0.0609	0.0021	596	17	585	12
50	132	79	0.60	n.d.	0.801	0.030	0.0954	0.0018	0.38	0.0609	0.0021	597	17	587	10
51	42	42	1.01	n.d.	0.787	0.031	0.096	0.003	0.20	0.0595	0.0032	589	18	590	16
52	202	69	0.34	n.d.	0.776	0.034	0.0959	0.0030	0.39	0.0586	0.0025	583	20	591	18
53	65	53	0.81	n.d.	0.814	0.031	0.0960	0.0017	0.36	0.0615	0.0022	605	18	591	10
54	75	68	0.91	n.d.	0.843	0.034	0.0961	0.0022	0.40	0.0636	0.0024	621	19	591	13
55	50	34	0.69	n.d.	0.923	0.047	0.0974	0.0022	0.29	0.0687	0.0034	664	25	599	13
56	81	60	0.73	n.d.	0.834	0.041	0.0980	0.0033	0.44	0.0617	0.0029	616	23	603	20
57	98	70	0.71	n.d.	0.830	0.033	0.0989	0.0023	0.36	0.0609	0.0023	614	18	608	13
58	25	18	0.70	n.d.	0.842	0.035	0.100	0.003	0.20	0.0610	0.0033	621	19	615	16
59	72	57	0.79	n.d.	0.832	0.034	0.1019	0.0023	0.36	0.0592	0.0023	615	19	626	14
60	49	15	0.30	n.d.	0.871	0.037	0.1030	0.0020	0.36	0.0613	0.0024	636	20	632	12
61	88	91	1.04	n.d.	4.980	0.283	0.3020	0.0126	0.34	0.1196	0.0069	1816	49	1701	63
62	246	153	0.62	n.d.	5.568	0.070	0.3269	0.0042	0.42	0.1235	0.0017	1911	11	1823	20
63	757	113	0.15	n.d.	5.743	0.255	0.3472	0.0076	0.35	0.1200	0.0051	1938	39	1921	37
64	520	70	0.14	n.d.	5.902	0.193	0.3482	0.0060	0.45	0.1229	0.0036	1962	29	1926	29
Sample 1B – Maslak															
1	244	185	0.76	638	0.430	0.010	0.0565	0.0007	0.16	0.0552	0.0013	363	7	354	4
2	108	73	0.68	n.d.	0.431	0.028	0.0572	0.0013	0.19	0.0546	0.0035	364	20	359	8
3	223	70	0.31	1315	0.645	0.013	0.0822	0.0009	0.06	0.0569	0.0013	506	8	509	5
4	66	55	0.83	>459	0.686	0.025	0.0841	0.0018	0.23	0.0591	0.0022	530	15	521	11
5	894	204	0.23	7338	0.714	0.070	0.0863	0.0084	0.47	0.0600	0.0060	547	43	534	50
6	62	37	0.59	>447	0.681	0.026	0.0865	0.0013	0.01	0.0571	0.0023	528	16	535	7
7	120	134	1.12	>1066	0.718	0.028	0.0875	0.0028	0.43	0.0595	0.0023	550	17	541	17
8	159	50	0.31	>1255	0.729	0.036	0.0887	0.0037	0.38	0.0596	0.0031	556	22	548	22
9	173	67	0.39	n.d.	0.716	0.036	0.0892	0.0021	0.25	0.0582	0.0029	548	22	551	13
10	162	70	0.43	n.d.	0.741	0.039	0.0910	0.0025	0.34	0.0591	0.0030	563	23	561	15
11	413	97	0.23	3631	0.737	0.011	0.0912	0.0007	0.10	0.0586	0.0010	561	6	563	4
12	86	67	0.78	n.d.	0.748	0.039	0.0928	0.0019	0.22	0.0585	0.0030	567	23	572	11
13	66	52	0.79	>568	0.834	0.023	0.0939	0.0010	0.01	0.0644	0.0020	616	13	579	6
14	322	102	0.32	n.d.	0.770	0.036	0.0948	0.0021	0.28	0.0589	0.0027	580	21	584	12
15	666	336	0.50	>5658	0.800	0.014	0.0949	0.0013	0.19	0.0611	0.0012	597	8	584	8
16	114	72	0.64	>920	0.800	0.020	0.0959	0.0014	0.08	0.0604	0.0017	597	11	591	8

Table 2. Continued.

No.	U ppm	Th ppm	Th/U ratio	$^{206}Pb/^{204}Pb$ ratio	$^{207}Pb/^{235}U$ ratio	1s	$^{206}Pb/^{238}U$ ratio	1s	σ	$^{207}Pb/^{206}Pb$ ratio	1s	$^{207}Pb/^{235}U$ Ma	1s	$^{206}Pb/^{238}U$ Ma	1s
17	74	62	0.84	n.d.	0.808	0.044	0.0966	0.0023	0.29	0.0607	0.0032	601	25	594	13
18	312	166	0.53	n.d.	0.781	0.037	0.0968	0.0021	0.31	0.0585	0.0027	586	21	596	12
19	63	45	0.72	n.d.	0.832	0.051	0.0969	0.0023	0.24	0.0623	0.0037	615	28	596	13
20	38	29	0.76	>329	0.805	0.033	0.0970	0.0016	0.15	0.0602	0.0025	600	18	597	10
21	146	76	0.52	n.d.	0.788	0.041	0.0971	0.0028	0.36	0.0588	0.0029	590	24	598	16
22	79	78	0.99	>788	0.785	0.021	0.0971	0.0010	0.01	0.0586	0.0017	589	12	598	6
23	38	32	0.84	n.d.	0.768	0.056	0.0973	0.0026	0.18	0.0572	0.0042	578	33	598	15
24	56	47	0.85	>476	0.811	0.026	0.0974	0.0012	0.07	0.0604	0.0020	603	15	599	7
25	34	21	0.63	n.d.	0.899	0.066	0.0975	0.0021	0.15	0.0669	0.0049	651	36	600	13
26	34	28	0.82	>323	0.791	0.038	0.0976	0.0024	0.22	0.0587	0.0028	592	22	600	14
27	31	21	0.68	>265	0.863	0.036	0.0978	0.0016	0.05	0.0640	0.0028	632	20	602	9
28	77	131	1.70	n.d.	0.836	0.044	0.0980	0.0020	0.21	0.0619	0.0033	617	25	603	12
29	232	8	0.04	1959	0.861	0.018	0.0985	0.0013	0.01	0.0634	0.0014	631	10	605	8
30	63	53	0.85	>595	0.837	0.025	0.0986	0.0014	0.18	0.0616	0.0019	618	14	606	8
31	83	87	1.05	n.d.	1.044	0.074	0.0988	0.0020	0.17	0.0767	0.0054	726	37	607	12
32	51	41	0.81	n.d.	0.804	0.052	0.0989	0.0022	0.20	0.0590	0.0038	599	29	608	13
33	43	34	0.80	>368	0.836	0.029	0.0990	0.0014	0.01	0.0612	0.0023	617	16	609	8
34	52	24	0.45	305	0.802	0.026	0.0991	0.0012	0.02	0.0587	0.0020	598	15	609	7
35	47	42	0.89	n.d.	0.875	0.054	0.0991	0.0023	0.24	0.0640	0.0039	638	30	609	13
36	61	57	0.92	>579	0.761	0.024	0.0991	0.0016	0.14	0.0557	0.0019	575	14	609	9
37	117	114	0.98	n.d.	0.808	0.041	0.0994	0.0025	0.31	0.0589	0.0029	601	23	611	15
38	56	34	0.61	438	0.814	0.023	0.0995	0.0013	0.01	0.0593	0.0018	605	13	612	7
39	111	88	0.79	>1069	0.825	0.021	0.0996	0.0016	0.13	0.0600	0.0017	611	12	612	9
40	79	73	0.92	n.d.	0.780	0.043	0.0998	0.0020	0.21	0.0567	0.0031	585	25	613	12
41	37	27	0.73	248	0.763	0.031	0.0998	0.0013	0.01	0.0554	0.0024	576	18	614	8
42	171	47	0.28	n.d.	0.777	0.089	0.1004	0.0106	0.44	0.0561	0.0066	584	52	617	62
43	288	244	0.85	>2702	0.846	0.025	0.1008	0.0026	0.49	0.0609	0.0017	622	14	619	15
44	50	33	0.66	>512	0.803	0.026	0.1008	0.0013	0.09	0.0577	0.0020	598	15	619	8
45	124	52	0.42	n.d.	0.817	0.042	0.1010	0.0021	0.26	0.0586	0.0029	606	24	620	12
46	47	25	0.53	n.d.	0.774	0.050	0.1014	0.0022	0.17	0.0554	0.0036	582	29	623	13
47	56	38	0.68	n.d.	0.828	0.056	0.1015	0.0043	0.29	0.0592	0.0041	612	32	623	25
48	292	120	0.41	n.d.	0.913	0.046	0.1015	0.0021	0.28	0.0652	0.0032	658	25	623	12
49	49	43	0.87	>467	0.794	0.027	0.1016	0.0015	0.04	0.0567	0.0021	593	16	624	9
50	123	114	0.93	>1142	0.850	0.026	0.1021	0.0023	0.18	0.0603	0.0021	624	14	627	14
51	80	27	0.34	>757	0.825	0.045	0.1030	0.0048	0.51	0.0581	0.0029	611	25	632	28
52	23	7	0.33	n.d.	0.938	0.070	0.1043	0.0028	0.18	0.0652	0.0049	672	37	640	16
53	197	31	0.15	>7833	6.413	0.095	0.3652	0.0036	0.05	0.1273	0.0022	2034	13	2007	17
54	62	73	1.18	>2687	10.942	0.351	0.4817	0.0140	0.51	0.1647	0.0050	2518	30	2535	61
55	88	81	0.92	n.d.	13.615	0.823	0.5169	0.0241	0.39	0.1910	0.0115	2723	59	2686	103
Sample 18 – Maslak															
1	725	63	0.09	>3696	0.395	0.010	0.0535	0.0015	0.84	0.0536	0.0008	338	8	336	9
2	465	280	0.60	2251	0.423	0.012	0.0580	0.0016	0.76	0.0529	0.0010	358	8	363	10
3	232	168	0.73	>1240	0.435	0.014	0.0581	0.0016	0.66	0.0543	0.0014	367	10	364	10
4	113	97	0.86	>598	0.473	0.023	0.0587	0.0019	0.43	0.0584	0.0026	393	16	368	11
5	76	50	0.67	>436	0.490	0.020	0.0597	0.0019	0.49	0.0595	0.0023	405	14	374	12
6	1251	627	0.50	6719	0.452	0.019	0.0604	0.0026	0.57	0.0542	0.0021	379	13	378	16
7	1899	1060	0.56	>11450	0.456	0.011	0.0622	0.0017	0.91	0.0532	0.0006	382	8	389	10
8	423	10	0.02	>2600	0.540	0.017	0.0686	0.0020	0.36	0.0570	0.0020	438	12	428	12
9	673	497	0.74	3969	0.660	0.018	0.0779	0.0022	0.80	0.0614	0.0011	515	11	484	13
10	248	55	0.22	>2009	0.700	0.038	0.0839	0.0045	0.01	0.0605	0.0034	539	23	520	27
11	295	163	0.55	>2341	0.654	0.018	0.0843	0.0023	0.79	0.0563	0.0010	511	11	522	14
12	132	177	1.34	>1027	0.701	0.031	0.0844	0.0033	0.60	0.0602	0.0023	539	19	522	20
13	169	137	0.81	1231	0.672	0.024	0.0848	0.0024	0.59	0.0574	0.0017	522	15	525	14
14	115	65	0.57	>891	0.877	0.041	0.0859	0.0030	0.54	0.0740	0.0030	639	22	531	18
15	234	74	0.32	>2053	0.754	0.020	0.0923	0.0020	0.19	0.0592	0.0018	571	11	569	12
16	92	95	1.03	478	0.971	0.048	0.0941	0.0036	0.56	0.0749	0.0031	689	25	580	21
17	355	167	0.47	>3222	0.787	0.024	0.0944	0.0029	0.76	0.0604	0.0013	589	14	582	17
18	149	182	1.22	>1464	0.793	0.022	0.0953	0.0018	0.22	0.0603	0.0018	593	13	587	11
19	393	166	0.42	2733	0.797	0.025	0.0972	0.0031	0.69	0.0595	0.0015	595	14	598	18
20	212	79	0.37	2063	0.805	0.027	0.0975	0.0031	0.71	0.0599	0.0015	599	15	600	18
21	72	66	0.93	>682	0.819	0.024	0.0976	0.0018	0.29	0.0608	0.0018	607	14	600	11
22	58	54	0.93	>497	0.821	0.035	0.0980	0.0028	0.47	0.0607	0.0023	609	20	603	16
23	154	74	0.48	>1411	0.840	0.030	0.0996	0.0035	0.69	0.0612	0.0017	619	16	612	21
24	91	83	0.92	510	0.951	0.042	0.0997	0.0036	0.50	0.0692	0.0028	679	22	613	21
25	45	38	0.84	>416	0.836	0.029	0.1008	0.0014	0.08	0.0601	0.0022	617	16	619	8
26	79	64	0.81	>766	0.838	0.030	0.1020	0.0029	0.57	0.0596	0.0018	618	17	626	17
27	67	26	0.39	>784	1.091	0.036	0.1140	0.0027	0.40	0.0694	0.0022	749	18	696	15
28	31	35	1.13	>918	6.484	0.131	0.3715	0.0052	0.29	0.1266	0.0027	2044	18	2036	25
29	96	33	0.34	>3375	6.462	0.096	0.3730	0.0037	0.14	0.1257	0.0021	2041	13	2043	17
30	108	86	0.80	>3712	6.722	0.373	0.3740	0.0210	0.53	0.1303	0.0071	2076	50	2048	99
31	255	160	0.63	>9606	7.994	0.210	0.4008	0.0115	0.81	0.1446	0.0025	2230	24	2173	53
32	71	37	0.53	>3005	7.496	0.219	0.4043	0.0122	0.83	0.1345	0.0023	2173	27	2189	56
33	392	93	0.24	>20666	13.064	0.296	0.5169	0.0135	0.95	0.1833	0.0016	2684	22	2686	58
34	100	4	0.04	>4780	14.807	0.640	0.5283	0.0211	0.46	0.2032	0.0088	2803	42	2734	90

1s – error of the values in the preceding column

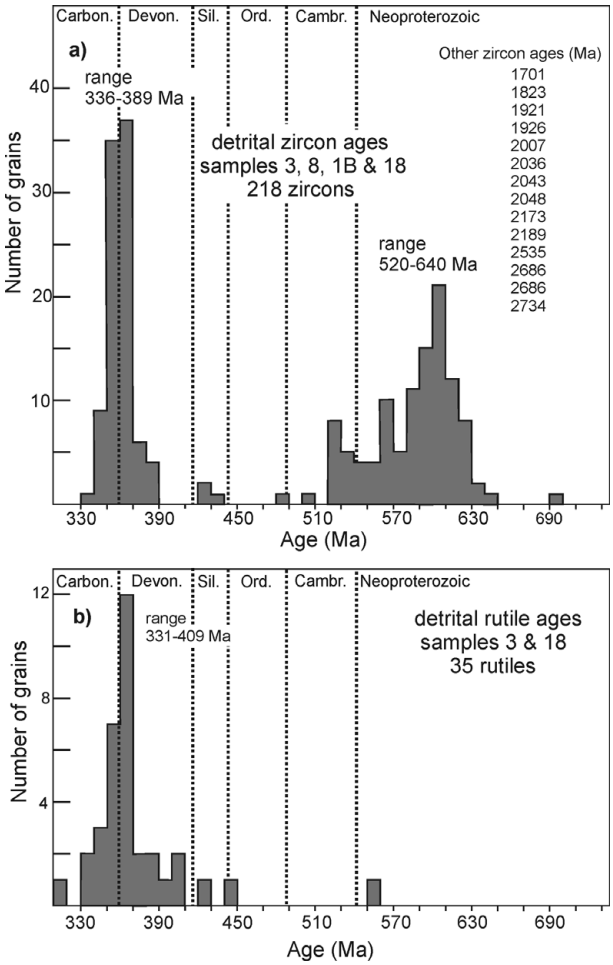

Figure 8. Histograms showing the age distribution of Palaeozoic–Neoproterozoic (a) detrital zircons from four Carboniferous sandstone samples and (b) detrital rutiles from two samples. The ages are grouped in 10 Ma intervals.

359 ± 5 and 357 ± 5 Ma, respectively (Fig. 12a, c). In contrast, the Cambrian–Neoproterozoic zircon ages are distributed between 520 Ma and 640 Ma, suggesting that the source rocks comprised magmatic protoliths of various ages. This is clear in Gebze-3, Scutaria-8 and Maslak-1B, where the Cambrian–Neoproterozoic zircons are spread out on the concordia (Fig. 12b, d, e).

Detrital rutile in sandstone is predominantly derived from medium- to high-grade metamorphic rocks and/or from recycled sediments (Force, 1980). Table 3 and Figure 8b give the U–Pb ages of 35 detrital rutiles from two sandstone samples (Gebze-3 and Maslak-18). They show a pronounced Late Devonian–Early Carboniferous age peak (368 ± 12 Ma,) with only one Neoproterozoic rutile. The concordia age of the sample Maslak-18 is 360 ± 4 Ma (Fig. 12f), coeval with the equivalent zircon ages from Gebze-3 and Scutaria-8 samples (Fig. 12a, c).

Coeval zircon and rutile ages indicate that the Late Devonian–Early Carboniferous metamorphism was closely associated with magmatism (Fig. 8). The age spectra of rutile and zircon can be best explained by a scenario where both minerals are from one localized area that has experienced one Late Devonian–Early Carboniferous metamorphic event (recorded by rutile) and several earlier magmatic periods and/or received sedimentary detritus (recorded by zircon) before this last metamorphic event. The older rutiles, if there were any, must have been overprinted by the Late Devonian–Early Carboniferous metamorphism. The well-defined rutile age peak, and the narrow time interval between the rutile ages and the depositional age of the Trakya Formation (*c*. 340–330 Ma), indicate that the cooling age of this metamorphic terrane was only slightly older than the deposition of the Trakya Formation.

7. Detrital zircon and rutile geochemistry

Figure 13 shows the REE patterns of the detrital zircons from two sandstone samples. Although the zircons are of various ages they all show enrichment in HREE, negative Eu and positive Ce anomalies, which are typical features of magmatic zircons. The Th/U ratios of zircons are between 0.3 and 0.9 (Table 2), characteristic, although not conclusive, for magmatic zircons (e.g. Teipel *et al.* 2004).

The trace element composition of detrital rutile can provide information on the nature of the protolith including the metamorphic facies and temperature of metamorphism in the source region (Zack, von Eynatten & Kronz, 2004; Triebold *et al*. 2007; Meinhold *et al.* 2008*a*). One hundred rutile grains from three sandstone samples (3, 18 and 1B) have been analysed for trace elements. The Zr concentrations in the detrital rutiles fall predominantly in the range 20–1000 ppm, Cr 10–1000 ppm, Nb 200–3100 ppm (Table 4). The Cr and Nb concentrations of detrital rutiles have been used to define the protolith (Zack, von Eynatten & Kronz, 2004; Triebold *et al*. 2007). Rutiles from three sandstone samples indicate a metamorphic provenance dominated by metapelitic rocks (Fig. 14).

Zirconium content of rutile has been suggested as a geothermometer by Zack, Moraes & Kronz (2004) based on the reaction:

$$ZrSiO_4(\text{zircon}) = ZrO_2(\text{in rutile}) + SiO_2(\text{quartz})$$

Zirconium contents of rutiles from three sandstone samples indicate a dominantly amphibolite-facies metamorphic provenance with metamorphic temperatures mostly in the range of of 550 to 750 °C (Fig. 14).

8. Discussion

8.a. Provenance

The sandstone framework petrography indicates a predominantly magmatic provenance for the siliciclastic turbidites of the Trakya Formation. The detrital zircon ages indicate that the magmatic rocks in the source region were Neoproterozoic (640 to 520 Ma) and Late Devonian to Early Carboniferous (390–335 Ma). Some of the Neoproterozoic magmatic clasts could have been

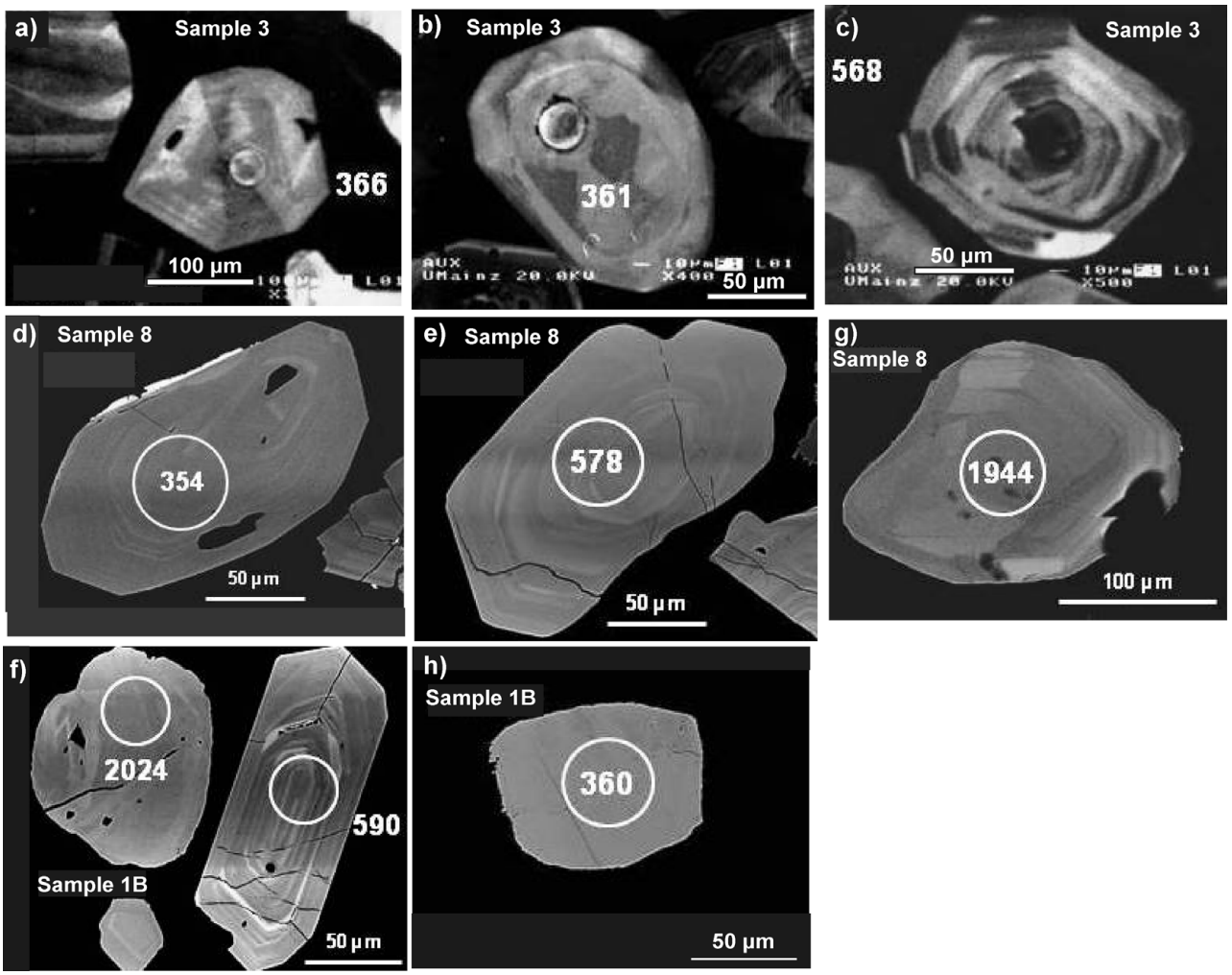

Figure 9. Cathode Luminescence and Back Scattered Electron images of some of the analysed zircons (a–g) and rutile (h). Note the euhedral to subhedral habits and sector and oscillatory zoning of the Late Devonian–Early Carboniferous (a, b, d) and Neoproterozoic (c, e, f) zircons indicating a magmatic protolith. The Palaeoproterozoic zircons, on the other hand, are rounded and have smoother zoning profiles (g, f).

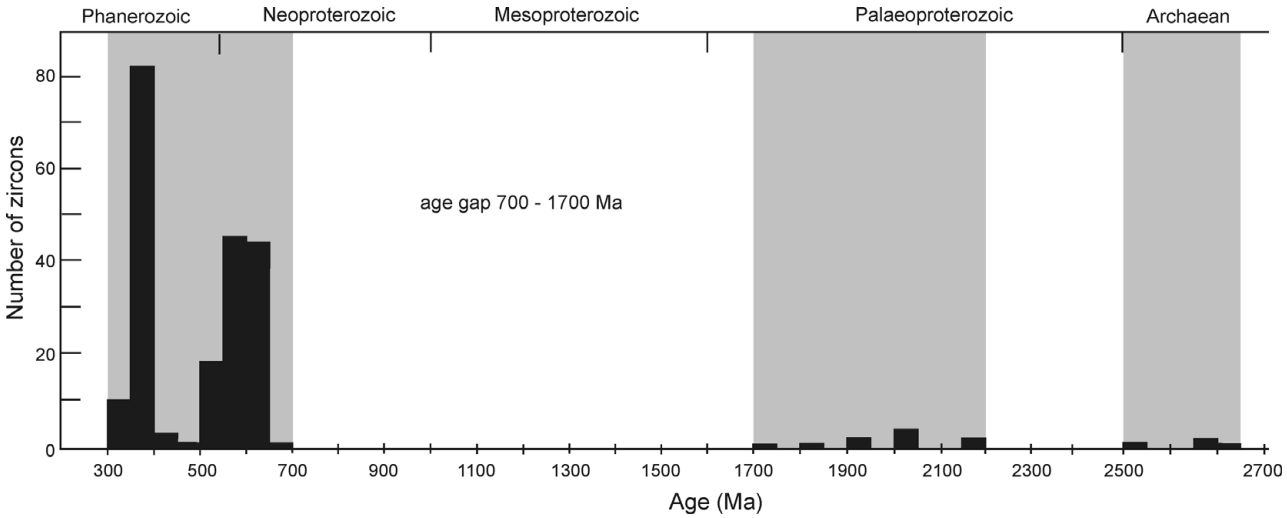

Figure 10. Histogram showing the age distribution of all the detrital zircons from four Carboniferous sandstone samples.

recycled from sedimentary rocks, however, the scarcity of sedimentary clasts in the Carboniferous sandstones make this a slight possibility. The metamorphic clasts are second in abundance in the Carboniferous sandstones; the geochemistry of the detrital rutiles and their isotopic ages indicate a metamorphic source of Upper Devonian–Lower Carboniferous amphibolite-facies metapelites and metabasites. The sedimentary clasts are rare, and carbonate clasts are virtually absent. The sandstone discrimination diagrams suggest that the

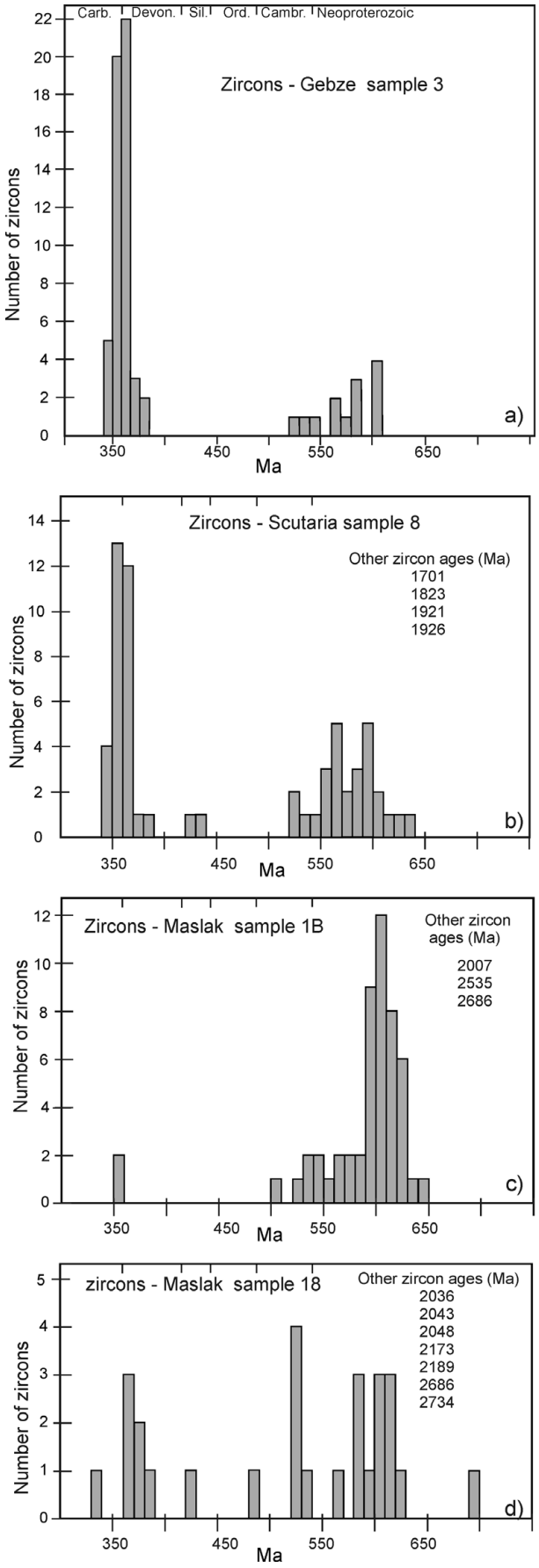

Figure 11. Histograms showing the age distribution of Palaeozoic–Neoproterozoic detrital zircons from four Carboniferous sandstone samples. Note the systematic change in zircon ages between the samples. The ages are grouped in 10 Ma intervals. For location of samples, see Figure 4.

Trakya Formation was being supplied from a dissected magmatic arc.

The scarcity of the sedimentary clasts and absence of carbonate fragments implies that the Palaeozoic series of the Istanbul Zone, which includes an 850 m thick Upper Silurian–Devonian carbonate sequence, was not a major source during Early Carboniferous times. The absence of Mesoproterozoic detrital zircons, recorded in the Ordovician quartzites of the Istanbul Zone (Ustaömer *et al*. 2010), also shows that the source of the Carboniferous sandstones was outside the Istanbul Zone. The virtual absence of Archaean to Palaeoproterozoic detrital zircons and abundance of the Neoproterozoic zircons exclude the Palaeoproterozoic (2300–2100 Ma) Ukranian shield (Baltica) north of the Black Sea as a source area (Bogdanova *et al.* 1996; Claesson *et al.* 2001).

Neoproterozoic (590–560 Ma) granitoids are widespread in Europe, extending from the Variscan massifs of central Europe through the Carpathians into the Pontides (e.g. Neubauer, 2002). The Neoproterozoic magmatism was produced in the Pan-African/Cadomian magmatic arcs, which characterize the northern margins of Gondwana (e.g. Stern, 1994) and hence Pan-African/Cadomian magmatism is widespread in the peri-Gondwana terranes including Avalonia and Armorican terrane assemblage (cf. Ustaömer *et al*. 2010). In contrast, Neoproterozoic granitoids are not known from the Sakarya Zone or from the Strandja Massif, and appear to be rare in Bulgaria and Greece (Carrigan *et al.* 2006; Sunal *et al*. 2008).

Late Devonian–Early Carboniferous magmatic and metamorphic rocks, a major source for the Lower Carboniferous flysch of the Istanbul Zone, are not known from the Eastern Mediterranean region and the Balkans (cf. fig. 10 of Meinhold *et al.* 2008*b*). The Variscan metamorphism in Bulgaria and in Turkey is of Late Carboniferous age (330–310 Ma, Okay *et al.* 1996; Okay, Satır & Siebel, 2006; Topuz *et al.* 2004, 2007; Velichkova *et al.* 2004). The Variscan plutonism in the same area is middle Carboniferous–Early Permian in age (320–270 Ma, Okay *et al.* 2001; Okay, Monod & Monié, 2002; Carrigan *et al.* 2005; Sunal *et al.* 2006, 2008; Topuz *et al.* 2007, 2010; Anders, Reischmann & Kostopoulos, 2007; Ustaömer, Ustaömer & Robertson, 2010) with the exception of one Early Devonian (*c.* 398 Ma) granitoid in NW Turkey (Çamlık granitoid in Fig. 1; Okay *et al.* 1996; Okay, Satır & Siebel, 2006). Sunal *et al*. (2008) report Early Carboniferous (*c*. 350 Ma) ages from the cores of Late Carboniferous zircons in the granitoids of the Strandja Massif. Such zircons are, however, absent in the Carboniferous metasediments of the Strandja Massif, indicating that such granitoids, if present, were not exposed in Early Carboniferous times.

Late Devonian to Early Carboniferous magmatism, although absent in the eastern Mediterranean, is widespread in the Armorican terranes such as the French Massif Central (Faure *et al.* 2005), the Mid-German Crystalline High (e.g. Anthes & Reischmann, 2001), the Bohemian Massif (Finger *et al.* 1997) and

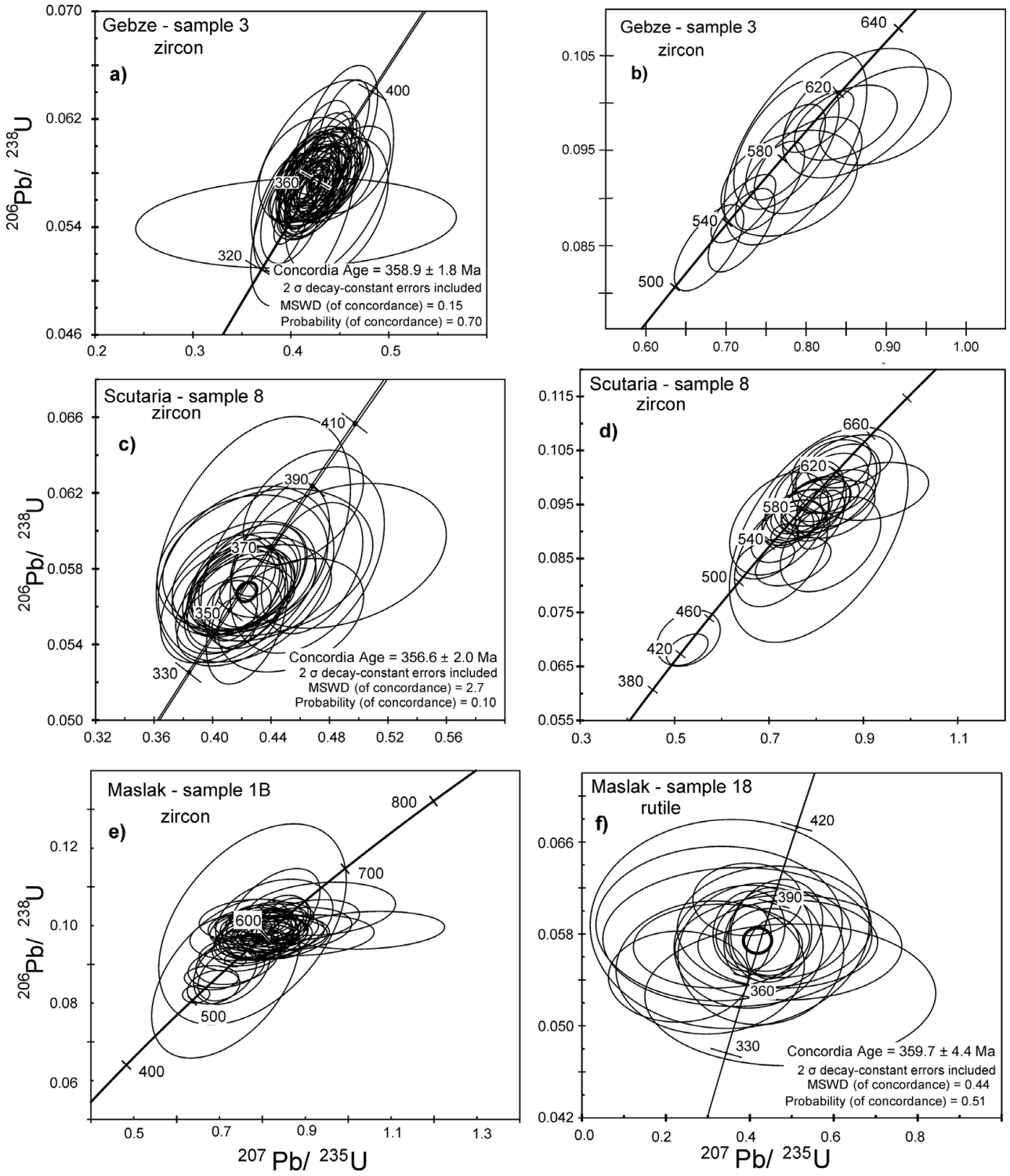

Figure 12. U–Pb Concordia diagrams of detrital zircons and rutiles from the Carboniferous flysch of the Trakya Formation. Data-point error elipses are 2 sigma. Please notice that errors used in the text are always ≥ 1.5 %, here 357 ± 5 Ma and 359 ± 5 Ma (see Section 6.a). For location of samples, see Figure 4.

the Tatra mountains in the western Carpathians (Poller *et al.* 2000). It is in generally calc-alkaline, intermediate to basic in chemistry and exhibits a significant mantle contribution (e.g. Shaw, Downes & Thirwall, 1993; Pin & Paquette, 2002); it is generally interpreted as having been produced during the southward subduction of the Rheic ocean. Late Devonian–Early Carboniferous metamorphism has also been described from the Variscan massifs of central Europe (e.g. Schulmann *et al.* 2005; Kroner *et al.* 2008; Poller *et al.* 2000).

8.b. Geological evolution of the Istanbul Zone

In terms of the crystalline basement, the Palaeozoic stratigraphy and palaeobiogeography, the Istanbul Zone is correlated with Avalonia, and the Intra-Pontide

Table 3. U–Pb isotope data from the detrital rutiles from the Carboniferous sandstones of the Istanbul Zone

No.	U ppm	Th ppm	Th/U ratio	$^{206}Pb/^{208}Pb$ ratio	$^{207}Pb/^{235}U$ ratio	1s	$^{206}Pb/^{238}U$ ratio	1s	σ	$^{207}Pb/^{206}Pb$ ratio	1s	$^{207}Pb/^{235}U$ Ma	1s	$^{206}Pb/^{238}U$ Ma	1s
Sample 3 – Gebze															
1	12	0.173	0.015	7	0.503	0.096	0.0584	0.0023	0.03	0.0625	0.0120	414	67	366	14
2	13	0.069	0.005	14	0.458	0.064	0.0607	0.0021	0.01	0.0547	0.0079	383	46	380	13
3	52	0.653	0.012	5	0.549	0.145	0.0706	0.0038	0.03	0.0563	0.0151	444	100	440	23
4	13	<0.034	<0.003	30	0.438	0.048	0.0647	0.0024	0.12	0.0491	0.0054	369	34	404	14
5	5	<0.034	<0.008	>12	0.499	0.141	0.0655	0.0034	0.04	0.0552	0.0158	411	101	409	21
6	9	0.060	0.007	8	0.620	0.122	0.0899	0.0032	0.01	0.0500	0.0100	490	79	555	19
7	7	<0.034	<0.005	12	0.384	0.083	0.0591	0.0020	0.01	0.0471	0.0103	330	63	370	12
8	9	0.43	0.050	2	0.199	0.144	0.0582	0.0020	0.01	0.0248	0.0179	184	129	364	12
Sample 18 – Maslak															
1	6	<0.031	<0.005	>9	0.497	0.142	0.0527	0.0025	0.02	0.0683	0.0197	409	101	331	15
2	40	0.027	0.001	>62	0.455	0.026	0.0567	0.0011	0.15	0.0582	0.0033	381	18	356	7
3	24	<0.030	<0.001	>37	0.449	0.041	0.0579	0.0017	0.06	0.0562	0.0052	376	29	363	10
4	23	0.049	0.002	>34	0.464	0.045	0.0586	0.0017	0.17	0.0575	0.0055	387	32	367	10
5	8	<0.033	<0.004	>15	0.426	0.081	0.0563	0.0025	0.03	0.0550	0.0106	361	59	353	15
6	7	<0.043	<0.006	>11	0.306	0.092	0.0551	0.0024	0.04	0.0402	0.0121	271	74	346	14
7	52	<0.027	<0.001	60	0.395	0.023	0.0574	0.0013	0.12	0.0498	0.0030	338	17	360	8
8	24	0.063	0.003	33	0.442	0.041	0.0575	0.0011	0.08	0.0558	0.0052	372	29	360	7
9	36	0.077	0.002	22	0.398	0.035	0.0583	0.0014	0.10	0.0495	0.0044	340	26	365	9
10	6	<0.034	<0.006	14	0.492	0.110	0.0568	0.0019	0.02	0.0628	0.0142	406	78	356	11
11	9	0.324	0.037	12	0.397	0.073	0.0569	0.0022	0.01	0.0506	0.0094	340	54	357	13
12	13	0.297	0.024	10	0.340	0.078	0.0501	0.0022	0.02	0.0492	0.0114	297	60	315	13
13	17	0.538	0.032	9	0.582	0.072	0.0678	0.0020	0.09	0.0623	0.0078	466	47	423	12
14	32	0.132	0.004	9	0.480	0.066	0.0580	0.0016	0.06	0.0600	0.0083	398	46	363	9
15	8	0.826	0.108	8	0.352	0.136	0.0589	0.0037	0.01	0.0434	0.0169	306	107	369	23
16	8	<0.033	<0.004	7	0.371	0.131	0.0577	0.0025	0.03	0.0465	0.0165	320	102	362	15
17	13	0.175	0.013	5	0.327	0.120	0.0589	0.0027	0.02	0.0402	0.0148	287	96	369	17
18	32	0.654	0.021	4	0.324	0.082	0.0569	0.0015	0.03	0.0413	0.0105	285	65	357	9
19	11	0.177	0.017	4	0.458	0.094	0.0587	0.0021	0.04	0.0567	0.0118	383	68	367	13
20	15	2.16	0.147	4	0.230	0.068	0.0543	0.0016	0.01	0.0308	0.0092	210	58	341	10
21	28	0.84	0.030	4	0.394	0.053	0.0610	0.0013	0.01	0.0469	0.0064	337	39	382	8
22	5	0.056	0.011	4	0.096	0.176	0.0597	0.0038	0.00	0.0116	0.0213	93	177	374	23
23	34	0.748	0.022	3	0.491	0.088	0.0571	0.0016	0.05	0.0623	0.0112	405	61	358	10
24	8	0.340	0.042	2	0.184	0.328	0.0537	0.0040	0.01	0.0249	0.0443	172	329	337	25
25	13	0.470	0.036	2	0.757	0.305	0.0632	0.0038	0.05	0.0869	0.0351	572	194	395	23
26	17	3.196	0.184	1	0.450	0.290	0.0573	0.0038	0.03	0.0570	0.0367	377	226	359	23
27	10	0.647	0.064	1	0.536	0.678	0.0541	0.0065	0.00	0.0718	0.0912	436	591	340	40

1s – error of the values in the preceding column

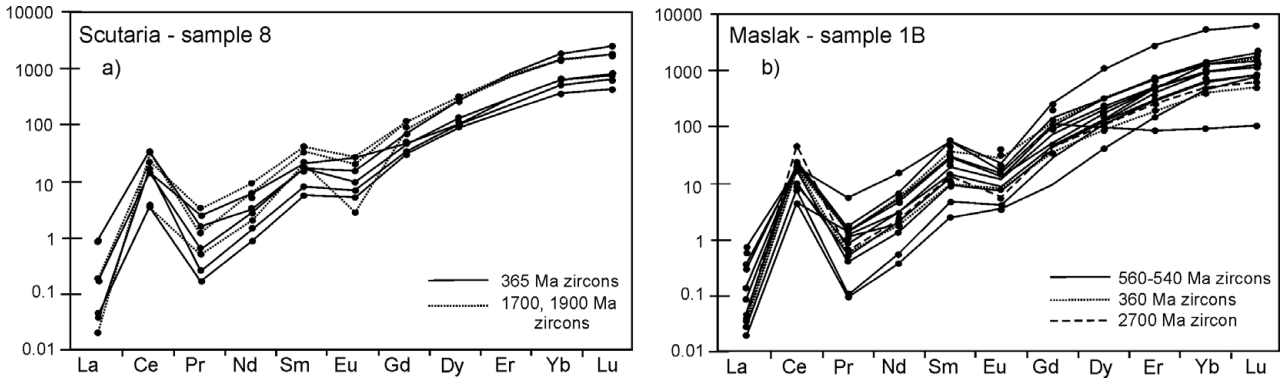

Figure 13. Primitive-mantle normalized incompatible element patterns of detrital zircons from the Carboniferous sandstone sample 8 (a) and 1B (b).

suture with the Rheic suture (Stampfli & Borel, 2002; Kalvoda *et al*. 2003; Okay, Satır & Siebel, 2006; Okay *et al.* 2008; Bozkurt *et al.* 2008; Sunal *et al*. 2008; Ustaömer *et al.* 2010). An Avalonian origin for the Istanbul Zone is also supported by the detrital zircons from the Ordovician and Silurian sandstones (Ustaömer *et al*. 2010), which show an absence of 2400 to 2050 Ma detrital zircons, a characteristic feature for Avalonia (Samson *et al*. 2005). In this context, the Trakya Formation can be compared with the coeval turbidites in the Rhenohercynicum, which have a similar mineralogical composition to those from the Trakya Formation, including an upward decrease in modal feldspar in sandstones (cf. Floyd *et al*. 1990).

Avalonia was accreted to the southern margin of Laurussia during Late Ordovician–Early Silurian times. Palaeomagnetic studies (Evans *et al*. 1991) indicate that in the Middle Silurian to Carboniferous interval, the Istanbul Zone was also located on the southern margin of Laurussia and was facing the Rheic

Table 4. Trace element concentrations of the detrital rutiles from the Carboniferous sandstones

No.	V ppm	Cr ppm	Zr ppm	Nb ppm	Sn ppm	Hf ppm	Ta ppm	W ppm	U ppm	T °C	log(Cr/Nb)
Sample 3 – Gebze											
1	880	771	323	226	8.8	14	10	37	7.9	655	0.53
2	1727	531	913	2449	98	48	126	80	10	748	−0.66
3	1457	577	665	2442	34	34	174	162	2.5	717	−0.63
4	689	642	339	2413	78	21	105	32	50	659	−0.57
5	550	458	448	1942	39	21	25	606	49	682	−0.63
6	599	268	191	644	13	8.7	42	152	6.2	614	−0.38
7	2660	889	428	1778	92	25	128	209	3.8	678	−0.30
8	704	425	156	2305	62	8.1	186	104	<0.13	599	−0.73
9	2290	700	436	1459	72	27	145	51	3.6	680	−0.32
10	3134	1486	881	209	8.5	24	9.5	5.9	6.6	744	0.85
11	1322	678	747	2898	76	42	142	111	5.7	728	−0.63
12	1194	55	98	243	<0.74	2.8	11	66	0.17	567	−0.64
13	547	86	317	7382	54	13	341	88	0.75	653	−1.93
14	1047	461	198	1673	93	8.5	133	106	2.2	616	−0.56
15	434	14	107	569	12	5.4	32	20	0.6	572	−1.61
16	1016	269	191	2345	52	8.4	225	136	4.9	614	−0.94
17	240	105	34	383	16	1.8	33	55	<0.15	502	−0.56
18	662	258	200	222	30	11	3.9	5.1	5.8	617	0.07
19	1219	436	234	1461	30	11	82	382	2.4	629	−0.53
20	1522	651	361	3392	36	17	353	132	1.8	664	−0.72
Sample 18 – Maslak											
1	849	590	90	1279	59	56	102	98	2.7	561	−0.34
2	1272	18	542	189	26	32	23	49	18	699	−1.01
3	740	254	610	450	19	37	24	12	7.8	709	−0.25
4	994	495	108	1360	58	25	104	100	1.6	573	−0.44
5	1179	405	180	1308	102	9	102	125	6.0	609	−0.51
6	1302	1434	216	2804	82	8	240	66	26	623	−0.29
7	1085	465	167	1945	60	23	156	395	2.3	604	−0.62
8	1136	34	167	68	4.4	6.1	3.0	17	0.23	604	−0.30
9	1428	74	289	466	29	14	39	59	5.5	646	−0.80
10	1471	130	139	1252	37	7.9	73	57	3.4	591	−0.99
11	2732	986	876	2470	119	43	127	110	12	744	−0.40
12	2461	570	316	1789	152	17	23	116	4.0	653	−0.50
13	1320	535	107	1391	76	6.9	96	96	1.8	573	−0.42
14	1771	482	330	2863	106	16	205	221	27	656	−0.77
15	2214	380	851	2509	134	37	76	89	23	741	−0.82
16	1517	522	984	1643	64	40	66	69	7.8	755	−0.50
17	895	220	676	1923	14	22	83	160	4.8	719	−0.94
18	907	878	443	593	7	15	25	40	2.9	681	0.17
19	1840	588	444	6414	59	38	546	259	7.8	681	−1.04
20	609	723	439	811	10	19	45	40	36	680	−0.05
21	2843	643	395	1446	36	18	42	35	6.5	671	−0.35
22	1971	439	553	1682	85	35	77	133	10	700	−0.58
23	1358	1382	311	4520	149	13	522	160	8.0	651	−0.51
24	1684	390	285	598	71	12	33	25	24	644	−0.19
25	2010	43	631	703	113	27	47	164	0.4	712	−1.21
26	1191	366	27	169	5.0	<1	7.6	70	0.2	488	0.33
27	4363	966	825	1176	136	36	32	126	4.5	738	−0.09
28	1824	537	442	4620	117	25	163	124	1.2	681	−0.93
29	1116	443	261	1309	117	13	90	177	22	638	−0.47
30	945	<16	352	1075	216	17	44	128	23	662	<−1.81
31	1252	59	356	1102	129	17	33	128	46	663	−1.27
32	1292	346	1039	1802	63	55	87	75	7.9	761	−0.72
33	1063	747	325	697	22	13	46	31	1.8	655	0.03
34	2380	721	695	6918	148	38	507	387	21	722	−0.98
35	1222	687	516	285	19	19	11	21	18	694	0.38
36	721	793	235	296	8.3	10	14	83	27	629	0.43
37	1693	621	420	3050	87	25	164	95	2.1	676	−0.69
38	1328	274	347	233	13	13	7.7	47	<0.2	661	0.07
39	1686	1175	495	1031	24	17	72	17	3.8	691	0.06
40	1009	53	456	706	35	23	21	33	7.3	683	−1.13
41	5401	362	1267	1362	191	50	81	73	18	781	−0.58
42	998	547	1572	2012	261	59	68	144	37	804	−0.57
43	1759	200	301	2802	124	14	135	215	12	649	−1.15
44	1013	110	363	297	7.8	21	14	45	<0.2	664	−0.43
45	1588	748	500	3107	97	25	195	153	10	691	−0.62
46	981	69	736	1422	57	30	55	76	21	727	−1.32
47	2406	1012	1027	4318	68	50	73	128	10	759	−0.63
48	1446	447	522	1167	207	29	151	106	24	695	−0.42
49	776	778	355	365	19	25	18	12	14	662	0.33
50	1822	560	469	5096	120	22	432	320	36	686	−0.96
51	735	447	248	645	38	16	24	17	3.7	634	−0.16
52	1231	1630	418	1726	125	15	65	87	38	676	−0.02

Table 4. Continued.

No.	V ppm	Cr ppm	Zr ppm	Nb ppm	Sn ppm	Hf ppm	Ta ppm	W ppm	U ppm	T °C	log(Cr/Nb)
Sample 1B – Maslak											
1	1096	109	343	496	28	19	47	41	0.26	659	−0.66
2	1021	155	332	646	20	12	35	167	3.50	657	−0.62
3	1067	675	153	1620	62	7.6	127	120	0.56	598	−0.38
4	744	449	123	1068	38	4.8	73	86	<0.12	582	−0.38
5	923	429	129	1052	36	4.9	69	155	<0.11	586	−0.39
6	815	615	32	252	3.8	1.5	17	181	<0.12	499	0.39
7	733	3116	1255	226	32	41	12	19	8.60	780	1.14
8	480	106	43	612	8.8	1.8	52	45	0.27	515	−0.76
9	1045	990	45	179	3.6	2.6	14	17	0.60	518	0.74
10	98	175	96	126	<1.19	7.9	41	10	0.54	565	0.14
11	904	433	43	180	5.3	4.3	11	174	0.16	515	0.38
12	837	457	103	1162	43	5.9	76	182	2.50	570	−0.40
13	893	1107	69	333	8.0	3.4	23	84	0.19	544	0.52
14	83	33	177	1198	7.5	22	48	35	<0.18	608	−1.56
15	1193	546	196	660	87	7.9	37	235	10	616	−0.08
16	801	484	35	519	21	1.4	41	19	<0.14	502	−0.03
17	722	365	123	672	32	8.4	57	71	0.37	582	−0.26
18	1018	473	192	3169	125	10	358	145	5.3	614	−0.83
19	634	190	22	790	28	0.92	60	49	0.21	477	−0.62
20	444	49	41	912	11	0.84	68	32	2.7	512	−1.27
21	475	299	43	1319	59	3.3	107	88	0.36	515	−0.64
22	1792	480	939	2418	105	44	94	165	17	750	−0.70
23	793	516	28	175	11	1.1	12	19	0.13	491	0.47
24	767	80	203	412	43	11	26	32	7.6	618	−0.71
25	281	389	128	530	8.0	11	18	19	0.15	585	−0.13
26	642	532	34	183	4.0	2.5	12	7.2	1.0	501	0.46
27	57	<6.69	140	651	5.2	11	62	80	1.6	591	<−1.99
28	67	13	298	721	1.1	17	71	393	4.8	648	−1.75
29	991	67	259	366	16	16	14	36	5.0	637	−0.74
30	535	116	27	844	19	1.1	66	23	0.17	489	−0.86
31	369	32	35	639	19	1.3	46	27	0.55	504	−1.30
32	2022	33	21	236	39	1.6	11	46	7.2	476	−0.85
33	689	227	36	332	19	2.3	15	470	1.2	505	−0.17

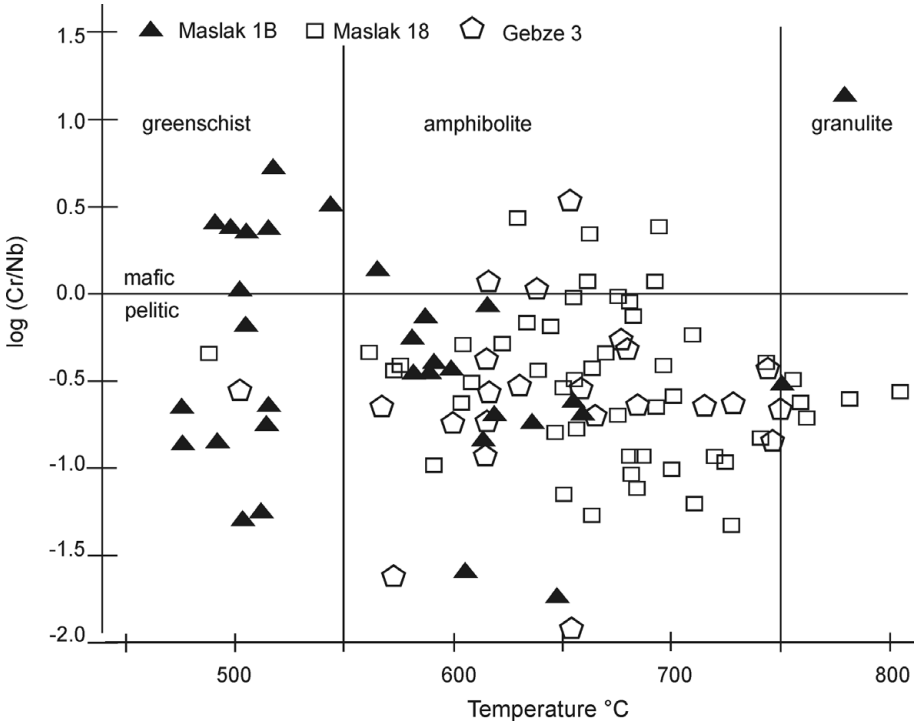

Figure 14. Geochemistry of the detrital rutiles. Metamorphic temperatures are calculated from the Zr contents of rutiles, using Tomkins, Powell & Ellis (2007) calibration for a pressure of 10 kbar. The log(Cr/Nb) axis after Triebold *et al*. (2007) provides an indication of the nature of the protolith (mafic or pelitic).

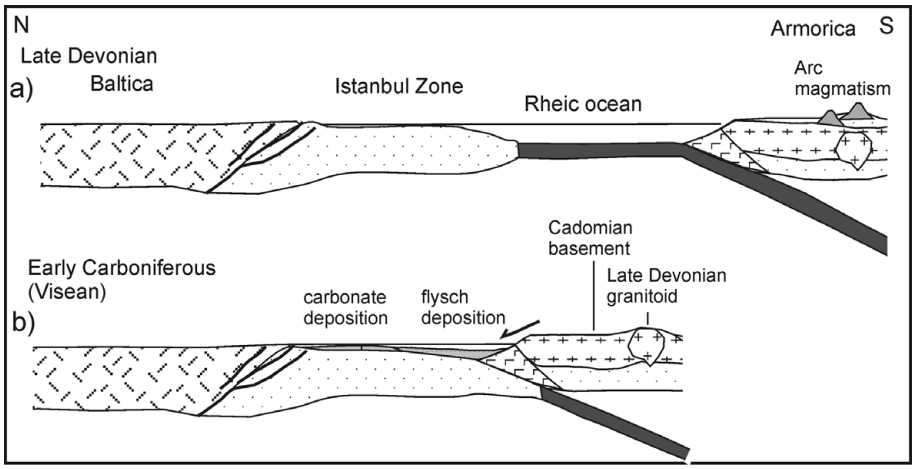

Figure 15. Schematic cross-sections depicting the geological evolution of the Istanbul Zone.

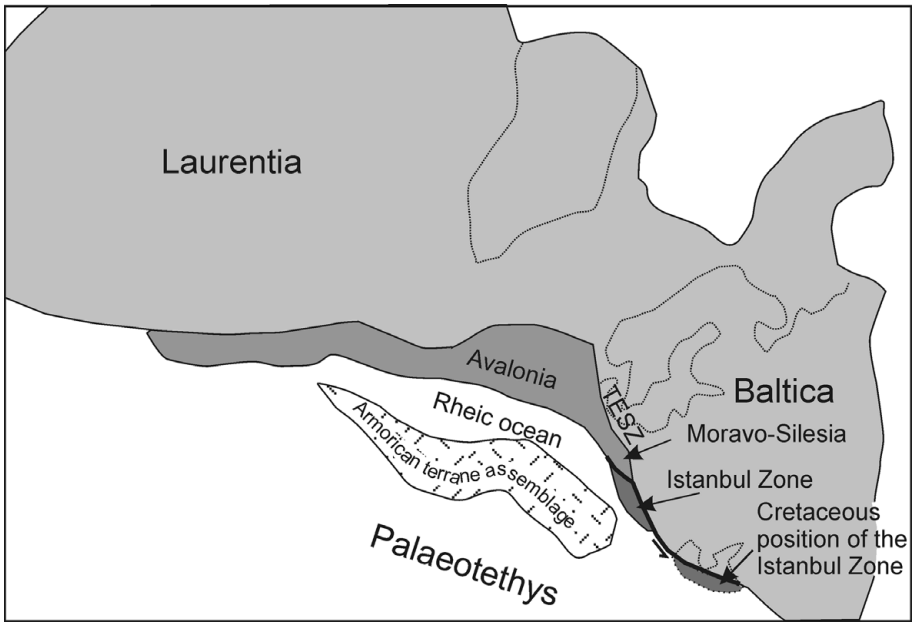

Figure 16. Early Carboniferous palaeogeography showing a possible location of the Istanbul Zone. TESZ – Trans-European suture zone.

ocean in the south (Fig. 15a). As the Istanbul Zone is free of Devonian or Carboniferous magmatism and has characteristics of a passive continental margin, the Rheic ocean must have been consumed by southward subduction, leading eventually to a collision with a Devonian–Carboniferous magmatic arc (Fig. 15b). The Carboniferous flysch of the Trakya Formation marks the onset of this collision, which must have been gentle, as it did not lead to deep burial and metamorphism of the Istanbul terrane.

The sandstone discrimination diagrams and detrital zircon ages indicate that the sandstones were supplied from a dissected magmatic arc of Late Devonian–Early Carboniferous age. The source region was devoid of Mesoproterozoic (1700–700 Ma) zircons, a characteristic feature of the Armorican terranes (Nance & Murphy, 1994; Linnemann *et al*. 2004; Ustaömer *et al*. 2010), which also comprise Late Devonian–Early Carboniferous magmatic rocks (e.g. Finger *et al*. 1997). These features indicate that the source of the Carboniferous flysch of the Istanbul Zone was a colliding Armorican terrane. As there are no Armorican terranes in the present vicinity of the Istanbul Zone, it must have been located during the Early Carboniferous close to the Armorican terrane assemblages, possibly the Bohemian Massif (Fig. 16). Avalonian terranes (e.g. Moravo-Silesia) east of the Bohemian Massif are stratigraphically similar to the Istanbul Zone, including the Visean flysch and the Upper Carboniferous coal measures (e.g. Narkiewics, 2007; Kalvoda *et al.* 2003, 2008). If this view is correct, then the Istanbul Zone must have been translated by strike-slip along the Trans-European suture zone (Fig. 16). Sinistral strike-slip has been independently postulated along this zone in the region of Dobrugea (e.g. Gradinaru, 1984; Seghedi, 2009). Banks & Robinson (1997) also postulated Early Jurassic sinistral displacement along the Trans-European suture zone. Although the precise location

of the Istanbul Zone during Carboniferous times is not known, geometrical constraints suggest that the total amount of slip along the Trans-European suture zone must have been at least several hundred kilometres.

By the Early Cretaceous the Istanbul Zone was situated on the southern margin of Laurasia between the Moesian and Scythian platforms (cf. Fig. 1; Okay, Şengör & Görür, 1994), from where it was displaced south to its present location with the Cretaceous opening of the West Black Sea basin. Therefore, the sinistral displacement of the Istanbul Zone must have occurred between Carboniferous and Early Cretaceous times, most likely in the Triassic–Early Cretaceous interval.

9. Conclusions

The Lower Carboniferous siliciclastic turbidites of the Istanbul Zone form an over 1500 m thick sequence marking the onset of the Variscan deformation. The sandstone framework petrography indicates that the source region consisted predominantly of intermediate volcanic and plutonic rocks and subordinate metamorphic rocks. Carbonate clasts are absent and sedimentary rock clasts are rare. Sandstone discrimination diagrams indicate a dissected magmatic arc as a source. Detrital zircon and rutile geochronology and geochemistry indicate a single source characterized by a Late Devonian to Early Carboniferous (390–335 Ma) magmatism and amphibolite-facies metamorphism with an overprinted Cambrian–Neoproterozoic (640 to 520 Ma) basement.

The Istanbul Zone is widely regarded as being part of the Avalonian terranes of central and western Europe. In the Silurian to Carboniferous, Avalonia formed part of the south-facing passive margin of Laurussia, which in the Early Carboniferous collided with the Armorican terranes leading to the Variscan orogeny. The Armorican terranes are characterized by the absence of Mesoproterozoic (700–1700 Ma) detrital zircons and by major Late Devonian–Early Carboniferous arc magmatism. The presence of magmatic clasts of Late Devonian–Early Carboniferous age and absence of Mesoproterozoic zircons in the Carboniferous flysch of the Istanbul Zone indicate a derivation from an Armorican terrane, especially since Late Devonian–Early Carboniferous magmatic and metamorphic rocks are not known in the eastern Mediterranean region. The stratigraphic similarities between the Istanbul Zone and the Avalonian terranes in eastern Europe, especially Moravo-Silesia in the Czech Republic, and the known strike-slip activity along the Trans-European suture zone, suggest that during Carboniferous times the Istanbul Zone was located further northwest, close to the Bohemian Massif, and has been translated by strike-slip movements into its Cretaceous location between Crimea and Moesia (Fig. 16).

Acknowledgements. We thank Gültekin Topuz and Burcu Altuntug for help with the samples. Aral Okay thanks the Turkish Academy of Sciences (TÜBA) for partial support. Thomas Zack thanks the German Science Foundation (DFG; grant Za285/7-1) and Geocycles for financial support. J. Kalvoda and an anonymous reviewer provided in-depth reviews, which improved the original manuscript.

References

AKSAY, A., PEHLIVAN, Ş., GEDIK, İ., BILGINER, E., DURU, M., AKBAŞ, B. & ALTUN, İ. 2002. *Geological map of Turkey, Zonguldak sheet, 1:500 000 scale*. Maden Tetkik ve Arama Enstitüsü, Ankara.

ANDERS, B., REISCHMANN, T. & KOSTOPOULOS, D. 2007. Zircon geochronology of basement rocks from the Pelagonian Zone, Greece: constraints on the pre-Alpine evolution of the westernmost Internal Hellenides. *International Journal of Earth Sciences* **96**, 639–61.

ANTHES, G. & REISCHMANN, T. 2001. Timing of granitoid magmatism in the eastern mid-German crystalline rise. *Journal of Geodynamics* **31**, 119–43.

BANKS, C. J. & ROBINSON, A. G. 1997. Mesozoic strike-slip back-arc basins of the western Black Sea region. In *Regional and Petroleum Geology of the Black Sea and Surrounding Region* (ed. A. G. Robinson), pp. 53–62. American Association of Petroleum Geologists, Memoir no. 68.

BLACK, L. P. & GULSON, B. L. 1978. The age of the Mud Tank carbonatite, Strangways Range, Northern Territory. *BMR Journal of Australian Geology and Geophysics* **3**, 227–32.

BOGDANOVA, S. V., PASHKEVICH, I. K., GORBATSCHEV, R. & ORLYUK, M. I. 1996. Riphean rifting and major Paleoproterozoic crustal boundaries in the basement of the East European Craton: geology and geophysics. *Tectonophysics* **268**, 1–21.

BOZKURT, E., WINCHESTER, J. A., YIGITBAŞ, E. & OTTLEY, C. J. 2008. Proterozoic ophiolites and mafic–ultramafic complexes marginal to the Istanbul Block: an exotic terrane of Avalonian affinity in NW Turkey. *Tectonophysics* **461**, 240–51.

BOZTUĞ, D. 1992. Lithostratigraphic units and tectonics of the southwestern part of Daday–Devrekani massif, western Pontides, Turkey. *Bulletin of the Mineral Research and Exploration, Turkey* **114**, 1–22.

ÇAPKINOĞLU, Ş. 2000. Late Devonian (Famennian) conodonts from Denizliköyü, Gebze, Kocaeli, northwestern Turkey. *Turkish Journal Earth Sciences* **9**, 91–112.

ÇAPKINOĞLU, Ş. 2005. Upper Devonian (upper Frasnian–lower Famennian) conodont biostratigraphy of the Ayineburnu formation (Istanbul Zone, NW Turkey). *Geologica Carpathica* **56**, 223–36.

CARRIGAN, C. W., MUKASA, S. B., HAYDOUTOV, I. & KOLCHEVA, K. 2005. Age of Variscan magmatism from the Balkan sector of the orogen, central Bulgaria. *Lithos* **82**, 125–47.

CARRIGAN, C. W., MUKASA, S. B., HAYDOUTOV, I. & KOLCHEVA, K. 2006. Neoproterozoic magmatism and Carboniferous high-grade metamorphism in the Sredna Gora Zone, Bulgaria: an extension of the Gondwana-derived Avalonia–Cadomian belt? *Precambrian Research* **147**, 404–16.

CHEN, F., SIEBEL, W., SATIR, M., TERZIOĞLU, N. & SAKA, K. 2002. Geochronology of the Karadere basement (NW Turkey) and implications for the geological evolution of the Istanbul Zone. *International Journal of Earth Sciences* **91**, 469–81.

CLAESSON, S., BOGDANOVA, S. V., BIBIKOVA, E. V. & GORBATSCHEV, R. 2001. Isotopic evidence for

Palaeoproterozoic accretion in the basement of the East European Craton. *Tectonophysics* **339**, 1–18.

DEAN, W. T., MONOD, O., RICKARDS, R. B., DEMIR, O. & BULTYNCK, P. 2000. Lower Palaeozoic stratigraphy and palaeontology, Karadere-Zirze area, Pontus Mountains, northern Turkey. *Geological Magazine* **137**, 555–82.

DICKINSON, W. R. 1970. Interpreting detrital modes of greywacke and arkose. *Journal of Sedimentary Petrology* **40**, 695–707.

DICKINSON, W. R., BEARD, L. S., BRAKENRIDGE, G. R., ERJAVEC, J. L., FERGUSON, R. C., INMAN, K. F., KNEPP, R. A., LINDBERG, F. A. & RYBERG, P. T. 1983. Provenance of North American Phaneorozoic sandstones in relation to tectonic setting. *Geological Society of America Bulletin* **94**, 222–35.

DIL, N. 1976. Assemblages charactéristiques de Foraminifères du Dévonien supérieur et du Dinantien de Turquie (bassin carbonifère de Zonguldak). *Annales de la Société géologique de Belgique* **99**, 373–400.

EVANS, I., HALL, S. A., SARIBUDAK, M. A. & AYKOL, A. 1991. Preliminary palaeomagnetic results from Palaeozoic rocks of the Istanbul–Zonguldak region, N.W. Turkey. *Bulletin of the Technical University of Istanbul* **44**, 165–90.

FAURE, M., BÉ MÉZÈME, E., DUGUET, M., CARTIER, C. & TALBOT, J. 2005. Paleozoic tectonic evolution of medio-Europa from the example of the French Massif Central and Massif Armoricain. *Journal of the Virtual Explorer*, Electronic Edition, vol. **19**, paper 5.

FINGER, E., ROBERTS, M. P., HAUNSCHMID, I. B., SCHERMAIER, A. & STEYRER, H. P. 1997. Variscan granitoids of central Europe: their typology, potential sources and tectonothermal relations. *Mineralogy and Petrology* **61**, 67–96.

FLOYD, P. A., LEVERIDGE, B. E., FRANKE, W., SHAIL, R. & DÖRR, W. 1990. Provenance and depositional environment of Rhenohercynian synorogenic greywackes from the Giessen Nappe, Germany. *Geologische Rundschau* **79**, 611–26.

FORCE, E. R. 1980. The provenance of rutile. *Journal of Sedimentary Petrology* **50**, 485–8.

GÖNCÜOĞLU, M. C., BONCHEVA, I. & GÖNCÜOĞLU, Y. 2004. First discovery of middle Tournaisian conodonts in the Griotte-type nodular pelagic limestones, Istanbul area, NW Turkey. *Rivista Italiana di Paleontologia e Stratigrafia* **110**, 431–9.

GÖRÜR, N., MONOD, O., OKAY, A. I., ŞENGÖR, A. M. C., TÜYSÜZ, O., YIĞITBAŞ, E., SAKINÇ, M. & AKKÖK, R. 1997. Palaeogeographic and tectonic position of the Carboniferous rocks of the western Pontides (Turkey) in the frame of the Variscan belt. *Bulletin de la Société géologique de France* **168**, 197–205.

GRADINARU, E. 1984. Jurassic rocks of north Dobrogea. A depositional–tectonic approach. *Revue Roumaine de Geologie, Geophysique et Geographie* **28**, 61–72.

GRADSTEIN, F. M., OGG, J. G., SMITH, A. G., BLEEKER, W. & LOURENS, L. J. 2004. A new geological time scale with special reference to Precambrian and Neogene. *Episodes* **27**, 83–100.

HAAS, W. 1968. Das Alt-Paläozoikum von Bithynien (Nordwest Türkei). *Neues Jahrbuch Geologische und Paleontologische Abhandlungen* **131**, 178–242.

HAYDOUTOV, I. & YANEV, S. 1997. The Protomoesian microcontinent of the Balkan Peninsula – a peri-Gondwanaland piece. *Tectonophysics* **272**, 303–13.

INGERSOLL, R. V. & SUCZEK, C. A. 1979. Petrology and provenance of Neogene sand from Nicobar and Bengal fans, DSDP sites 211 and 218. *Journal of Sedimentary Petrology* **49**, 1217–28.

INGERSOLL, R. V., BULLARD, T. F., FORD, R. L., GRIMM, J. P., PICKLE, J. D. & SARES, S. W. 1984. The effect of grain size on detrital modes: a test of the Gazzi–Dickinson point-counting method. *Journal of Sedimentary Petrology* **54**, 103–16.

JACKSON, S. E., PEARSON, N. J., GRIFFIN, W. L. & BELOUSOVA, E. A. 2004. The application of laser ablation-inductively coupled plasma-mass spectrometry to in situ U–Pb zircon geochronology. *Chemical Geology* **211**, 47–69.

KALVODA, J., LEICHMANN, J., BABEK, O. & MELICHAR, R. 2003. Brunovistulian Terrane (Central Europe) and Istanbul Zone (NW Turkey): Late Proterozoic and Paleozoic tectonostratigraphic development and paleogeography. *Geologica Carpathica* **54**, 139–52.

KALVODA, J., BABEK, O., FATKA, O., LEICHMANN, J., MELICHAR, R., NEHYBA, S. & SPACEK, P. 2008. Brunovistulian terrane (Bohemian Massif, Central Europe) from late Proterozoic to late Paleozoic: a review. *International Journal of Earth Sciences* **97**, 497–518.

KALVODA, J. & BÁBEK, O. 2010. The Margins of Laurussia in Central and Southeast Europe and Southwest Asia. *Gondwana Research* **17**, 526–45.

KAYA, O. 1969. Karbon bei Istanbul. *Neues Jahrbuch Geologische und Paleontologische Monatshefte 1969* **3**, 160–73.

KAYA, O. 1971. The Carboniferous stratigraphy of Istanbul (in Turkish). *Türkiye Jeoloji Kurumu Bülteni* **14**, 143–99.

KAYA, O. & MAMET, B. 1971. Biostratigraphy of the Visean Cebeciköy limestone near Istanbul, Turkey. *Journal of Foraminiferal Research* **1**, 77–81.

KEREY, I. E. 1984. Facies and tectonic setting of the Upper Carboniferous rocks of northwestern Turkey. In *The Geological Evolution of the Eastern Mediterranean* (eds J. E. Dixon & A. H. F. Robertson), pp. 123–8. Geological Society of London, Special Publication no. 17.

KEREY, I. E., KELLING, G. & WAGNER, R. H. 1986. An outline stratigraphy and palaeobotanical records from the middle Carboniferous rocks of northwestern Turkey. *Annales de la Société géologique du Nord* **CV**, 203–16.

KETIN, İ. 1983. *A general view of the geology of Turkey*. Istanbul Teknik Üniversitesi Matbaası, Istanbul, 596 pp. (in Turkish).

KRONER, U., MANSY, J.-L., MAZUR, S., ALEKSANDROWSKI, P., MANN, H. P., HUCKRIEDE, H., LACQUEMENT, F., LAMARCHE, J., LEDRU, P., PHARAOH, T. C., ZEDLER, H., ZEH, A. & ZULAUF, G. 2008. Variscan Tectonics. In *The Geology of Central Europe Volume 1: Precambrian and Palaeozoic* (ed. T. McCann), pp. 599–665. Geological Society of London.

LINNEMANN, U., MCNAUGHTON, N. J., ROMER, R. L., GEHMLICH, M., DROST, K. & TONK, C. 2004. West African provenance for Saxo-Thuringia (Bohemian Massif): Did Armorica ever leave pre-Pangean Gondwana? – U/Pb-SHRIMP zircon evidence and the Nd-isotopic record. *International Journal of Earth Sciences* **93**, 683–705.

LOBOZIAK, S. & DIL, N. 1973. Sur l'age Westphalien inferieur des couches de charbon sous la faille du Midi de la galerie – 200/34400A des mines de Çaydamar (Turquie) d'apres leur etude palynologique (microspores et megaspores). *Review of Palaeobotany and Palynology* **15**, 287–99.

LUVIZOTTO, G. L., ZACK, T., TRIEBOLD, S. & VON EYNATTEN, H. 2009. Rutile occurrence and trace element behavior in medium-grade metasedimentary rocks: example from

the Erzgebirge, Germany. *Mineralogy and Petrology* **97**, 233–49.

MEINHOLD, G., ANDERS, B., KOSTOPOULOS, D. & REISCHMANN, T. 2008*a*. Rutile chemistry and thermometry as provenance indicator: an example from Chios Island, Greece. *Sedimentary Geology* **203**, 98–111.

MEINHOLD, G., REISCHMANN, T., KOSTOPOULOS, D., LEHNERT, O., MATUKOV, D. & SERGEEV, S. 2008*b*. Provenance of sediments during subduction of Palaeotethys: detrital zircon ages and olistolith analysis in Palaeozoic sediments from Chios Island, Greece. *Palaeogeography, Palaeoclimatology, Palaeoecology* **263**, 71–91.

NANCE, R. D. & MURPHY, J. B. 1994. Contrasting basement isotopic signatures and the palinspastic restoration of peripheral orogens: example from the Neoproterozoic Avalonian–Cadomian belt. *Geology* **22**, 617–20.

NARKIEWICZ, M. 2007. Development and inversion of Devonian and Carboniferous basins in the eastern part of the Variscan foreland (Poland). *Geological Quarterly* **51**, 231–56.

NEUBAUER, F. 2002. Evolution of late Neoproterozoic to early Paleozoic tectonic elements in Central and Southeast European Alpine mountain belts: review and synthesis. *Tectonophysics* **352**, 87–103

NOBLE, P. J., TEKIN, U. K., GEDIK, İ. & PEHLIVAN, Ş. 2008. Middle to Upper Tournaisian radiolaria of the Baltalimani Formation, Istanbul, Turkey. *Journal of Paleontology* **82**, 37–56.

OKAY, A. C. 1947. Geologische und petrographische Untersuchung des Gebietes zwischen Alemdağ, Karlıdağ und Kayışdağ in Kocaeli, Bithynien, Türkei. *Istanbul Üniversitesi Fen Fakültesi Mecmuası, Seri B* **12**, 269–88.

OKAY, A. I. & TÜYSÜZ, O. 1999. Tethyan sutures of northern Turkey. In *The Mediterranean Basins: Tertiary Extension Within the Alpine Orogen* (eds B. Durand, L. Jolivet, F. Horváth & M. Séranne), pp. 475–515. Geological Society of London, Special Publication no.156.

OKAY, A. I., ŞENGÖR, A. M. C. & GÖRÜR, N. 1994. Kinematic history of the opening the Black Sea and its effect on the surrounding regions. *Geology* **22**, 267–70.

OKAY, A. I., SATIR, M., MALUSKI, H., SIYAKO, M., MONIE, P., METZGER, R. & AKYÜZ, S. 1996. Paleo- and Neo-Tethyan events in northwest Turkey: geological and geochronological constraints. In *Tectonics of Asia* (eds A. Yin & M. Harrison), pp. 420–41. Cambridge University Press.

OKAY, A. I., SATIR, M., TÜYSÜZ, O., AKYÜZ, S. & CHEN, F. 2001. The tectonics of the Strandja Massif: Variscan and mid-Mesozoic deformation and metamorphism in the northern Aegean. *International Journal of Earth Sciences* **90**, 217–33.

OKAY, A. I., MONOD, O. & MONIÉ, P. 2002. Triassic blueschists and eclogites from northwest Turkey: vestiges of the Paleo-Tethyan subduction. *Lithos* **64**, 155–78.

OKAY, A. I., SATIR, M. & SIEBEL, W. 2006. Pre-Alpide orogenic events in the Eastern Mediterranean region. In *European Lithosphere Dynamics* (eds D. G. Gee & R. A. Stephenson), pp. 389–405. Geological Society of London, Memoir no. 32.

OKAY, A. I., BOZKURT, E., SATIR, M., YIĞITBAŞ, E., CROWLEY, Q. G. & SHANG, C. K. 2008. Defining the southern margin of Avalonia in the Pontides: geochronological data from the Late Proterozoic and Ordovician granitoids from NW Turkey. *Tectonophysics* **461**, 252–64.

PAECKELMANN, W. 1938. Neue Beitrage zur Kenntnis des Geologie, Palaontologie und Petrographie der Umgegend von Konstantinople 2. Geologie Thraziens, Bithyniens und der Prinzeninseln. *Abhandlungen der preussische geologische Landesanstalt N.F.* **168**, 202 pp., Berlin.

PETTIJOHN, F. J., POTTER, P. E. & SIEVER, R. 1987. *Sand and Sandstone*, 2nd ed. Springer-Verlag, 553 pp.

PHARAOH, T. C. 1999. Palaeozoic terranes and their lithospheric boundaries within the Trans-European Suture Zone (TESZ): a review. *Tectonophysics* **314**, 17–41.

PIN, C. & PAQUETTE, J-L. 2002. Le magmatisme basique calcoalcalin d'âge dévono-dinantien du nord du Massif Central, témoin d'une marge active hercynienne: arguments géochimiques et isotopiques Sr:Nd. *Geodinamica Acta* **15**, 63–77.

POLLER, U., JANAK, M., KOHUT, M. & TODT, W. 2000. Early Variscan magmatism in the Western Carpathians: U–Pb zircon data from granitoids and orthogneisses of the Tatra Mountains (Slovakia). *International Journal of Earth Science* **89**, 336–49.

RUTTEN, M. G. 1969. *The Geology of Western Europe*. Amsterdam: Elsevier Publishing Company, 520 pp.

ŞAHIN, S. Y., GÜNGÖR, Y., AYSAL, N. & ÖNGEN, S. 2009. Geochemistry and SHRIMP zircon U–Pb dating of granitoids within the Strandja and İstanbul Zones (NW Turkey). *Abstracts, 62nd Geological Congress of Turkey*, Ankara, pp. 598–9.

SAMSON, S. D., D'LEMOS, R. S., MILLER, B. V. & HAMILTON, M. A. 2005. Neoproterozoic palaeogeography of the Cadomia and Avalon terranes: constraints from detrital zircon U–Pb ages. *Journal of the Geological Society, London* **162**, 65–71.

SCHÄFER, J., NEUROTH, H., AHRENDT, H., DÖRR, W. & FRANKE, W. 1997. Accretion and exhumation at a Variscan active margin, recorded in the Saxothuringian flysch. *Geologische Rundschau* **86**, 599–611.

SCHULMANN, K., KRÖNER, A., HEGNER, E., WENDT, I., KONOPASEK, J., LEXA, O. & STIPSKA, P. 2005. Chronological constraints on the pre-orogenic history, burial and exhumation of deep-seated rocks along the eastern margin of the Variscan orogen, Bohemian Massif, Czech Republic. *American Journal of Science* **305**, 407–48.

SHAW, A., DOWNES, H. & THIRLWALL, M. F. 1993. The quartz-diorites of Limousin: elemental and isotopic evidence for Devono-Carboniferous subduction in the Hercynian belt of the French Massif Central. *Chemical Geology* **107**, 1–18.

SEGHEDI, A. 2009. Paleozoic terrane accretion and Mesozoic evolution of the NW margin of the Black Sea. *Abstracts, 2nd International Symposium on the Geology of the Black Sea Region*, Ankara, pp. 178–9.

SLAMA, J., KOSLER, J., CONDON, D. J., CROWLEY, J. L., GERDES, A., HANCHAR, J. M., HORSTWOOD, M. S. A., MORRIS, G. A., NASDALA, L., NORBERG, N., SCHALTEGGER, U., SCHOENE, B., TUBRETT, M. N. & WHITEHOUSE, M. J. 2008. Plesovice zircon – a new natural reference material for U–Pb and Hf isotopic microanalysis. *Chemical Geology* **249**, 1–35.

STAMPFLI, G. M. & BOREL, G. D. 2002. A plate tectonic model for the Paleozoic and Mesozoic constrained by dynamic plate boundaries and restored synthetic oceanic isochrons. *Earth and Planetary Science Letters* **196**, 17–33.

STERN, R. J. 1994. Arc assembly and continental collision in the Neoproterozoic East African Orogen. *Annual Reviews of the Earth and Planetary Sciences* **22**, 319–51.

SUNAL, G., NATAL'IN, B., SATIR, M. & TORAMAN, E. 2006. Paleozoic magmatic events in the Strandja Masif, NW Turkey. *Geodinamica Acta* **19**, 283–300.

SUNAL, G., SATIR, M., NATAL'IN, B. & TORAMAN, E. 2008. Paleotectonic position of the Strandja Massif and surrounding continental blocks based on zircon Pb–Pb age studies. *International Geology Review* **50**, 519–45.

TAIT, J. A., BACHTADSE, V., FRANKE, W. & SOFFEL, H. C. 1997. Geodynamic evolution of the European Variscan Foldbelt: palaeomagnetic and geological constraints. *Geologische Rundschau* **86**, 585–98.

TEIPEL, U., EICHHORN, R., LOTH, G., ROHRMÜLLER, J., HÖLL, R. & KENNEDY, A. 2004. U–Pb SHRIMP and Nd isotopic data from the western Bohemian Massif (Bayerischer Wald, Germany): implications for Upper Vendian and Lower Ordovician magmatism. *International Journal of Earth Sciences* **93**, 782–801.

TOMKINS, H. S., POWELL, R. & ELLIS, D. J. 2007. The pressure dependence of the zirconium-in-rutile thermometer. *Journal of Metamorphic Geology* **25**, 703–13.

TOPUZ, G., ALTHERR, R., KALT, A., SATIR, M., WERNER, O. & SCHWARTZ, W. H. 2004. Aluminous granulites from the Pulur Complex, NE Turkey: a case of partial melting, efficient melt extraction and crystallization. *Lithos* **72**, 183–207.

TOPUZ, G., ALTHERR, R., SCHWARTZ, W. H., DOKUZ, A. & MEYER, H.-P. 2007. Variscan amphibolites-facies rocks from the Kurtoğlu metamorphic complex (Gümüşhane area, Eastern Pontides, Turkey). *International Journal of Earth Sciences* **96**, 861–73.

TOPUZ, G., ALTHERR, R., SIEBEL, W., SCHWARZ, W. H., ZACK, T., HASÖZBEK, A., BARTH, B, SATIR, M. & ŞEN, C. 2010. Carboniferous high-potassium I-type granitoid magmatism in the Eastern Pontides: the Gümüşhane pluton (NE Turkey). *Lithos* **116**, 92–110.

TRIEBOLD, S., VON EYNATTEN, H., LUVIZOTTO, G. & ZACK, T. 2007. Deducing source rock lithology from detrital rutile geochemistry: an example from the Erzgebirge, Germany. *Chemical Geology* **244**, 421–36.

TÜRKECAN, A. & YURTSEVER, A. 2002. *Geological map of Turkey, Istanbul sheet 1:500 000 scale*. Maden Tetkik ve Arama Enstitüsü, Ankara.

USTAÖMER, P. A. & ROGERS, G. 1999. The Bolu Massif: remnant of a pre-Early Ordovician active margin in the west Pontides, northern Turkey. *Geological Magazine* **136**, 579–92.

USTAÖMER, P. A., MUNDIL, R. & RENNE, P. R. 2005. U/Pb and Pb/Pb zircon ages for arc-related intrusions of the Bolu Massif (W Pontides, NW Turkey): evidence for Late Precambrian (Cadomian) age. *Terra Nova* **17**, 215–23.

USTAÖMER, P. A., USTAÖMER, T., GERDES, A. & ZULAUF, G. 2010. Detrital zircon ages from a Lower Ordovician quartzite of the Istanbul exotic terrane (NW Turkey): evidence for Amazonian affinity. *International Journal of Earth Sciences*, DOI: 10.1007/s00531-009-0498-1, in press.

USTAÖMER, P. A., USTAÖMER, T. & ROBERTSON, A. H. F. 2010. Ion Probe U–Pb dating of the Central Sakarya basement: a peri-Gondwana terrane cut by late Lower Carboniferous subduction/collision related granitic magmatism. *Geophysical Research Abstracts* **12**, EGU 2010-5966.

VELICHKOVA, S. H., HANDLER, R., NEUBAUER, F. & IVANOV, Z. 2004. Variscan to Alpine tectonothermal evolution of the Central Srednogorie unit, Bulgaria: constraints from Ar-40/Ar-39 analysis. *Schweizerische Mineralogische und Petrographische Mitteilungen* **84**, 133–51.

VERMEESCH, P. 2004. How many grains are needed for a provenance study? *Earth and Planetary Science Letters* **224**, 441–51.

WIEDENBECK, M., ALLE, P., CORFU, F., GRIFFIN, W. L., MEIER, M., OBERLI, F., VON QUADT, A., RODDICK, J. C. & SPEIGEL, W. 1995. 3 natural zircon standards for U–Th–Pb, Lu–Hf, trace-element and REE analyses. *Geostandards Newsletter* **19**, 1–23.

YIĞITBAŞ, E., KERRICH, R., YILMAZ, Y., ELMAS, A. & XIE, Q. L. 2004. Characteristics and geochemistry of Precambrian ophiolites and related volcanics from the Istanbul–Zonguldak Unit, Northwestern Anatolia, Turkey: following the missing chain of the Precambrian South European suture zone to the east. *Precambrian Research* **132**, 179–206.

YILMAZ, I. 1977. The absolute age and genesis of the Sancaktepe granite (Kocaeli peninsula) (in Turkish). *Türkiye Jeoloji Kurumu Bülteni* **20**, 17–20.

ZACK, T., VON EYNATTEN, H. & KRONZ, A. 2004. Rutile geochemistry and its potential use in quantitative provenance studies. *Sedimentary Geology* **171**, 37–58.

ZACK, T., MORAES, R. & KRONZ, A. 2004. Temperature dependence of Zr in rutile: empirical calibration of a rutile thermometer. *Contributions to Mineralogy and Petrology* **148**, 471–88.

ZACK, T., STOCKLI, D. F., LUVIZOTTO, G. L., BARTH, M. G., BELOUSOVA, E., WOLFE, M. R. & HINTON, R. W. In press. In-situ U/Pb rutile dating by LA-ICP-MS: ^{208}Pb correction and prospects for geological applications. *Contributions to Mineralogy and Petrology*.

ZAPCI, C., AKYÜZ, H. S. & SUNAL, G. 2003. An approach to the structural evolution of the Istanbul Zone. In *Proceedings of the Symposium on the Geology of the Istanbul Region*, pp. 5–14. Istanbul (in Turkish).